Department of Precision and Microsystems Engineering

Thermal Modelling of a Concept for a Hybrid Micro Combustion Generator

Florian Böhme

Report no	: 2022.085
Coach	: Dr.ir. J.F.L. Goosen
Professor	: Dr.ir. J.F.L. Goosen
Specialisation	: Mechatronic System Design (MSD)
Type of report	: Master Thesis
Date	: 29.11.2022

TU Delft Delft University of Technology

Challenge the future

Contents

Acronyms

EGR Exhaust Gas Recirculation. 7, 17–21, 26, 28, 33, 34, 36, 38–41, 43, 46, 47, 50, 51, 57, 59, 60

FWMAV Flapping Wing Micro Air Vehicles. 3, 5–7, 9, 13, 14, 18, 19, 21, 46, 47, 49, 55, 57, 59, 60

HCCI Homogeneous Charge Compression Ignition. 10, 13

IoT Internet of Things. 3, 5, 49, 55, 57

MAVs Micro Air Vehicles. 5, 6

MEMS Micro Electro Mechanical Systems. 31

MICE Micro Internal Combustion Engines. 7, 11–16, 21, 47, 57, 60, 63–65

MICSE Micro Internal Combustion Swing Engines. 13, 14

MTEG Micro Thermoelectric Generator Systems. 11, 12, 14, 21, 57

MTPV Micro Thermophotovoltaic Systems. 11, 12, 14, 21

TE Thermoelectric. 3, 7, 11, 12, 14–21, 23, 24, 27, 30–36, 38–41, 43, 44, 46, 47, 49, 51, 53, 57, 59, 60, 63–65

TPV Thermophotovoltaic. 11, 15, 16, 18, 20, 63–65

1

Abstract

Mobile electronics or remote devices like sensors for the Internet of Things (IoT) require energy storage with increasing energy densities, approaching the limits of the widespread lithium batteries. At the same time, lithium batteries are subject to growing criticism about their environmental impact due to their raw materials and their mining methods. Chemical energy seems to be a promising alternative and the development of micro combustion to make use of it is already for almost 30 years the topic of ongoing research. Recent studies show that compliant combustion engines are a good solution to mitigate some problems like leakage and friction and thus, achieve higher efficiencies. However, the most prevalent problem is heat losses through the walls because of the high surface-to-volume ratio in small-scale combustion. In this work, a design concept was proposed that not only insulates the compliant combustion chamber of the actuator for Flapping Wing Micro Air Vehicles (FWMAV) but also uses the waste heat to generate electricity. That was done by attaching Thermoelectric (TE) modules to a support structure and thermally connecting them with porous media to the oscillating combustor wall. The actuator uses the heat and pressure generated by the catalytic reaction of hydrogen peroxide and therewith, only emits steam and oxygen. With the help of a one-dimensional steady-state heat resistance model and a one-dimensional transient heat resistance-capacitance model, an optimum design was found. With that, it is possible to create a temperature difference sufficient enough to enable energy harvesting by TE modules. That was achieved by implementing an exhaust gas recirculation which transfers heat to the modules and simultaneously serves as a heating blanket for the combustor. A downside of the design is the relatively long time it takes to reach its steady state and especially for FWMAV, the increase in weight.

2

Introduction

Combustion-based small-scale power generators have been a part of research since the 90s and gain a lot more importance since modern applications require high energy-dense storage and current technologies like lithium batteries impose a lot of stress on the environment. More people than ever possess an increasing number of electronic devices, transportation is being electrified and the use of renewable energies requires storage to stabilize the grid in times of low power generation. The demand for lithium batteries and their questionably obtained raw materials is ever-increasing and pushes the industry into considering the use of controversial methods like deep-sea mining. If the boundaries for analyzing the ecological balance of a system are expanded in a way that the entire supply chain is included, many systems considered to be environmentally friendly or carbon-neutral turn out to be the opposite. To take the pressure off the market for lithium batteries and to improve the ecological balance it is important to develop sustainable alternatives that make use of socio-economically non-critical materials. One of these solutions is chemical energy storage. Compared to electrochemical batteries chemical fuel has a higher energy density which is especially important for small-scale applications where weight is a deciding factor. Examples are portable electronics or Micro Air Vehicles (MAVs) where miniaturization is a key element of new developments. Another advantage of chemical storage is that the stored energy stays the same while batteries discharge over time. In addition, charging times would be reduced to a minimum because the fuel could just be replaced. At first, combustion processes as a sustainable alternative to batteries seem counter-intuitive, however, the fuel suitable for use is not limited to hydrocarbons which indeed would end up as greenhouse gases. The products of combusting hydrogen peroxide produced with renewable energies would only be water and oxygen which enables indoor use in close proximity to people. Having these clear advantages in mind, a lot of current research focuses on omitting the downsides of such systems. The major problem of micropower generation is the suffering of heat losses so high that stable combustion can often not be guaranteed or that the low efficiencies obliterate the high energy densities of the fuel. Not only are these losses caused by the high surface-to-volume ratio but also by frictional and leakage losses that become more dominant the smaller the system's size is.

2.1. Flapping Wing Micro Air Vehicles

Micro power generators are very versatile and thus interesting for a variety of applications. Their different types can be optimized for delivering mechanical thrust for satellites, generating electrical power for portable electronics or remote sensors in industry 4.0 and Internet of Things (IoT) applications. Since all types of generators have similar problems and come down to a similar structure, results are easily transferable. An application that is especially feasible as a use case is MAVs, in particular, Flapping Wing Micro Air Vehicles (FWMAV) because of the high demands on size, weight and power output. Research on this type of air vehicle has the goal of further decreasing their size and weight to open up even more possibilities and applications in different sectors. Right now, most vehicles are still based on energy storage in lithium batteries that become a large portion of the overall weight and limit the miniaturization due to their low energy densities. If higher efficiencies for small-scale combustion could be achieved, generators could be produced on silicon carbide wafers with the help of semiconductor manufacturing [18]. Applications for these small aircraft could be anything in indoor environments, not accessible to humans, or in general very crowded surroundings [55]. That could be for example chemical plants to conduct measurements in polluted areas or greenhouses to

pollinate crops in a highly efficient and controllable way [66]. A resulting requirement for the MAVs is a high manoeuvrability and efficient flight to achieve a long flight duration. Flapping wing mechanisms are therefore attractive for these kinds of air vehicles since they are considered to create relatively high lift for their size and they can generate lift, thrust and control moments without additional actuators [55]. In addition, they can be operated at the resonance frequency of the body, an idea also originating from mimicking insects and birds [62]. Another important requirement is having no emissions to enable indoor usage. That includes not only noise but also exhaust gases dangerous for humans or the operating environment. That in turn implies constraints for the choice of an actuator for such MAVs. Whitney et al. developed a methodology for a conceptual design and show how to calculate the size of an actuator for an FWMAV. By including power electronics or amplifier circuitry, they showed that there is a critical wing radius that cannot be exceeded, even though bigger wings would lead for example to higher lift and payload. This critical radius is defined by the energy density of the actuator technology and takes also battery mass into account [65]. Also acknowledging the fact that the FWMAV become lighter and hence, more efficient, the more fuel is used, chemical power generators for delivering the power of such a vehicle seem to be a feasible alternative to conventional actuators. At TU Delft the DelFly (see Figure 2.2) is being developed and despite limiting the work in the corresponding book to batteries and electric motors, the potential of chemical actuators and their high energy density has been noted. Further, chemical actuation is said to possibly be the future for small FWMAVs while pointing out the disadvantage of still requiring an additional electric power source for onboard sensors and control equipment [12]. It could be a starting point for further research to develop a system that can combine a chemical actuator and an electrical power generator to omit this problem. Another research group at TU Delft, also mentioned in that book, is working on a chemical actuator for the Atalanta project to develop a butterfly-like drone at a small scale [3][57][30][27].

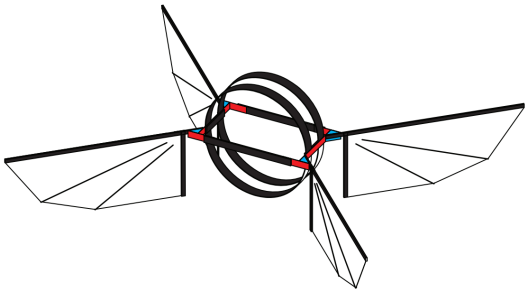

Figure 2.1: Concept of the wing actuation mechanism by Bolsman [6]

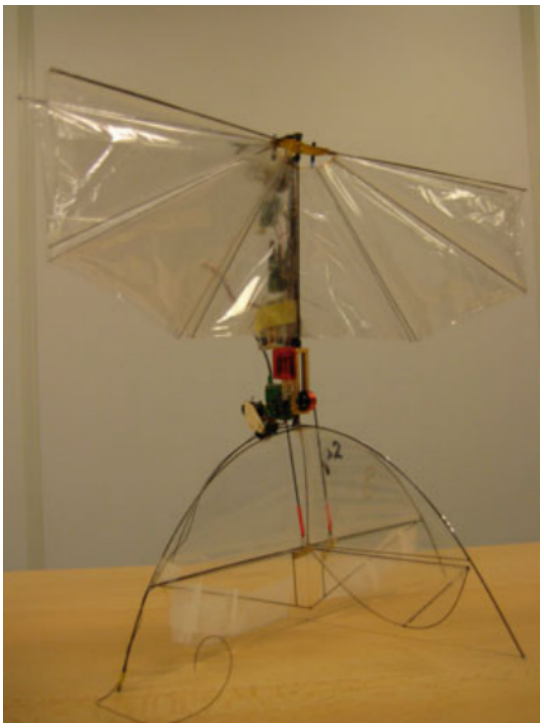

Figure 2.2: 'Standing tail' design of the DelFly [11]

As mentioned before, this project is also the study case for this work and further developments are going to be based on the actuator developed by Guido Mous which is presented in a later chapter. For the missions that this FWMAV is supposed to carry out, different requirements have been defined. These include autonomous flight, being able to hover and fly in a slow manner, communicating with others and a base station, as well as manage its power storage. In addition, it should provide a payload capacity and be adaptable for a variety of situations [6]. Despite the plan to design the mechanism with a low power consumption based on resonance and compliant structures, batteries and conventional actuators like a motor or a voice coil actuator would

not be able to power the air vehicle for a sufficient time. What the wing actuation mechanism and the entire concept of the FWMAV look like was mainly determined by the work of Bolsman and can be seen in [6]. The mentioned requirements for the Atalanta project result in different constraints for the actuator design. Because of all the above-mentioned points, an actuator for an FWMAV was chosen to be the orientation for this work in order to quantify the specifications of the system to be analyzed. That makes this research part of the described Atalanta project and the search for an actuator to power that drone for a flight time of at least 10 minutes. Nevertheless, as can be later seen, the results of this work, related to FWMAV, which seems like a small niche, can be applied to various other applications.

2.2. Aim of the research

The goal of this research is to develop a concept for generating electricity from the heat losses of Micro Internal Combustion Engines (MICE) by using TE modules. By that, the research question of whether TE modules can generate a notable amount of electrical power and thus, increase the efficiency of a MICE shall be answered. A numerical model of the system is built to analyze the effects of different configurations including the use of Exhaust Gas Recirculation (EGR). The focus lies on finding the configuration resulting in a relevant power output from the TE module while increasing the efficiency of the combustion chamber by insulating it. Finally, recommendations and design guidelines for such a hybrid system are developed.

2.3. Thesis Outline

The topic of the study is approached by the proposal of a mechanical design of the system in chapter 3 which is based on a state-of-the-art analysis of micropower generation and its problems. In that way, groundwork regarding the geometrical and material properties for the next step, a one-dimensional steady-state model, is laid. All underlying equations for the heat resistances and how each component is set up in that model are described in chapter 4. This chapter also includes the verification of the model and a thorough analysis of sensitivities and interdependencies. Based on the results, a design optimized for the electricity generation of the TE modules is developed. In chapter 5 a one-dimensional transient resistance-capacitance model is created to find out how the temperatures in the system change over time. Although each chapter has its own examination, in chapter 6 the general relevance of the results is discussed. Finally, in chapter 7 all findings are summarized in a conclusion and recommendations for further research are given.

3

Mechanical Design

3.1. Introduction

Before setting up a model, a design of the system needs to be developed that serves as a baseline for subsequent parameter changes. At first, previous design choices regarding the actuator are examined to then review different alternatives for implementing electricity generation. Section 3.3 summarizes choices and designs from previous research regarding energy storage and actuator types for powering an FWMAV. Relevant energy storage materials can be divided into two general subgroups, the chemical and electrochemical energy types. Earlier research regarding this topic showed, that chemical energy storage materials have a far higher energy density, also referred to as specific energy, as opposed to electrochemical ones, which are mainly used in conventional batteries [17]. A higher energy density means less weight and therefore better flight endurance for the FWMAV.
Similar counts for the types of actuators which can be split up into the groups of chemical and mechanical actuators. For electrical actuators, the stored energy (chemical or electrochemical) needs to be converted into electrical energy first, before it can be converted to mechanical energy. Every conversion step is subject to conversion losses, which makes the use of electrical actuators inefficient [12]. That is why it was decided in the research projects, on which this study is based, to focus on chemical energy storage in combination with chemically powered actuation [3][57][30][27].

3.2. Chemical Energy Storage

Table 3.1 shows the specific energies for certain storage materials [12][52]. As mentioned earlier, the specific energy of electrochemical storage is lower than the one of chemical. From an energy density point of view, it seems reasonable to choose hydrogen as a fuel since it has the highest density on the list. However, also other characteristics of the fuel play an important role in their feasibility for FWMAV. These include for instance availability or actuator choice but also emissions. Since the Atalanta is also supposed to fly inside and in close proximity to humans, the chosen fuel is not allowed to have harmful emissions. Nevertheless, the fuel has to generate gas during the reaction due to the plan of transforming chemical directly into mechanical energy. After weighing the pros and cons, Meskers proposed to use hydrogen peroxide for further research [3].

3.2.1. Hydrogen Peroxide

Hydrogen peroxide is a widespread chemical that is, due to its oxidizing capabilities, used for numerous applications like bleaching, cleaning or disinfecting, which makes it easily commercially available [44]. Its decomposition into water and oxygen under the generation of gas and heat is described by the following chemical equation.

$$2H_2O_2 \longrightarrow 2H_2O + O_2 \tag{3.1}$$

The reaction is influenced by temperature, pH and the impurity of the hydrogen peroxide [25]. Hydrogen Peroxide with a purity of 100% is not available which makes it necessary to know which substances, for example, stabilizers the solution contains. Otherwise, accumulation of these particles and in turn clogging of the catalyst or similar is possible [3].

Storage Material	Energy Type	Specific Energy [kJ/kg]
Hydrogen (compressed at 70 MPa)	Chemical	142000
LPG (including Propane /Butane)	Chemical	46400
Gasoline (petrol) / Diesel / Fuel oil	Chemical	46000
Jet fuel	Chemical	43000
Hydrogen peroxide	Chemical	2600
Hydrogen Fuel Cell	Electrochemical	2400
Lithium SOCl2	Electrochemical	1800
Formic Acid Fuel Cell	Electrochemical	1500
Lithium SOCl2 (high current)	Electrochemical	1100
Lithium-Sulphur batteries	Electrochemical	900
Alkaline batteries	Electrochemical	670
Lithium-ion polymer batteries	Electrochemical	650
Lithium-ion polymer batteries (small)	Electrochemical	450
Nickel-metal hydride batteries	Electrochemical	360
Lead-acid battery	Electrochemical	170

Table 3.1: Selection of different energy storage materials with their energy type and specific energy

	H_2O_2 strength (wt%)		
Property	35	50	70
Density at 20°C (g/cm^3)	1.1312	1.1953	1.2886
Viscosity at 20°C (mPa s)	1.11	1.17	1.23
Freezing Point (°C)	-33	-52.2	-40.3
Boiling Point (°C)	107.9	113.8	125.5

Table 3.2: Properties of hydrogen peroxide depending on the purity of the solution

In Table 3.2 important chemical properties of hydrogen peroxide solutions, depending on their purity, are listed [25]. 98% is the maximum achievable purity for hydrogen peroxide. For the actuator, higher hydrogen peroxide concentrations are important due to their higher energy density and higher reaction rate [3].

3.2.2. Catalyst

Many concepts for ignition mechanisms were reviewed to find the most suitable one for the special requirements. It has to be energy efficient but most importantly it needs to be able to ignite reliably without thermal quenching, which is one of the major problems in small-scale combustion engines or actuators. Among the concepts were for instance a glow plug, Homogeneous Charge Compression Ignition (HCCI) or catalytic materials. It was chosen to pursue a concept with a catalytic decomposition due to being passive and omitting the problem of quenching [27]. Catalysis describes the presence of a substance during a chemical reaction that is not used during the reaction but leads to an acceleration of it [53]. Catalytic reactions are divided into homogeneous and heterogeneous catalysis. The first is defined by reactants and a catalyst in the same chemical phase whereas the latter describes the reaction of reactants under the presence of a catalyst in a different phase [53]. From that, three combinations of reactants and catalysts follow, solid - solid, non-solid - solid, and non-solid - non-solid. The more area of the catalyst comes into contact with the reactant, the higher the reaction rate. Other factors that influence the speed of the catalytic reaction are temperature, pH, contamination and UV light [3]. The decomposition of hydrogen peroxide is catalyzed by metals like manganese, silver, platinum or gold [53]. Meskers showed in his research by conducting an experiment that manganese oxide is a suitable catalyst. Since the mixing of fluids in microstructures is a problem, it was decided to use a solid catalyst for the non-solid reactant hydrogen peroxide [3]. Manganese was on the edge of being classified as a critical raw material in the EU in 2020 and has questionable extraction methods, thus, a reevaluation of catalytic materials might be a topic for further research [20].

3.3. Small Chemical Engines

Research on small-scale engines started in the 1990s when Epstein et al. developed micro gas turbines at MIT. The hope was, and is until this day, to build generators with a high energy density for a great range of

applications in propulsion or portable power generation [18]. Since then a lot of micro-generators and small-scale engines were derived to introduce an often more sustainable alternative to batteries. The concepts developed roughly in the three main branches, MTPV, MTEG, and MICE [14].

3.3.1. Definition of Micro Combustion

In Table 3.3 it becomes visible that there are different definitions of micro- and mesoscale, which are often overlapping. Simplified the flame-quenching diameter means the minimum diameter of the combustion chamber necessary to enable stable combustion despite phenomena like heat loss to the walls. If the diameter of the combustion chamber is smaller than the flame-quenching diameter, the temperature inside the chamber does not exceed the minimum temperature required for stable combustion. As we can see later, the actuator this work is based on, is in the microscale region, following the physical length and the device scale definition since its cylinder has a length of 4.32 mm [27]. However, there could easily be micro air vehicles that would require an actuator with a length of above 10 mm, which would count as a mesoscale actuator based on the physical length definition. As opposed to that, based on the device scale definition, it would still count as microscale because it would be far smaller than conventional engine sizes for aircraft.

Definition based on	Combustion regime	Length Scale
Physical length	Mesoscale	1 - 10 mm
	Microscale	1 - 1000 μm
Flame-quenching diameter	Mesoscale	Combustor size larger than quenching diameter
	Microscale	Combustor size smaller than quenching diameter
Device Scale	Mesoscale	Larger than conventional engine size
	Microscale	Smaller than conventional engine size

Table 3.3: Definitions of micro- and mesoscale for micro combustion engines [36]

3.3.2. Micro Thermo Photovoltaic Systems (MTPV)

The basic principle of an MTPV is based on using photovoltaic cells to generate electricity from the emitted heat of a combustion engine. The device consists of four main components, a heat source (combustion chamber), which is encased in a cylindrical emitter, a dielectric filter and a low bandgap photovoltaic cell array (mostly GaSb) [23][64]. The system is not based on any moving parts, which is why it is considered to have high reliability [72]. The Thermophotovoltaic (TPV) cells can make use of light with wavelengths between 400 nm to 1.8 μm, whereas the broadband emitter also emits photons with a lower wavelength. These photons do not lead to any electricity generation but to a heating up of the TPV cell, which decreases its conversion efficiency. Therefore, the dielectric filter is used to not let these photons pass but even reflect them to recycle [73]. If not a broadband emitter is used but a selective emitter which only emits photons in the near-infrared range, then a filter is not necessary [14]. How the performance of the GaSb cell changes with regard to its temperature was researched by Ferguson and Fraas [21]. A low bandgap TPV cell requires a uniform temperature distribution over its entire area to achieve high efficiencies [23]. For that reason, different combustor configurations and shapes were tried to manipulate the flame anchoring point and the gas flow [5][73]. Figures 3.1 and 3.2 depict how the MTPV system from Chia and Feng looks in longitudinal and cross-section to make the working principle of such a generator clearer [8]. Modern MTPV reaches usually overall system efficiencies of around 6% which is mostly due to the high heat losses in the combustion chamber and the low conversion efficiencies of the TPV modules [74].

3.3.3. Micro Thermoelectric Generator Systems (MTEG)

The structure of a system to convert heat to electrical energy with Thermoelectric (TE) modules seems similar to using TPV cells. However, while the combustion chamber is comparable, a filter or an emitter is not needed since the TE modules work best with conduction whereas the TPV cells work best with radiation. The function of the TE modules is based on the Seebeck effect, which describes the causing of an electric current by a temperature difference between two junctions of two dissimilar conductors in a loop [54]. Since TE modules are sensitive to high temperatures, these systems operate at much smaller temperatures than TPV modules. This allows using them together with catalytic combustion which works at lower temperatures than flame combustion. Subsequently, the use of TE modules together with catalytic combustion makes it possible to use a larger variety of materials because the property of being heat resistant is no longer necessary

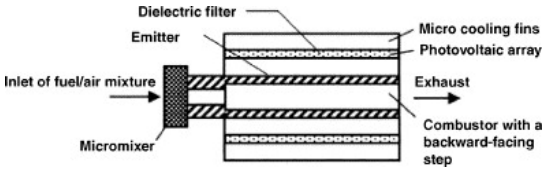

Figure 3.1: MTPV system in longitudinal section [8]

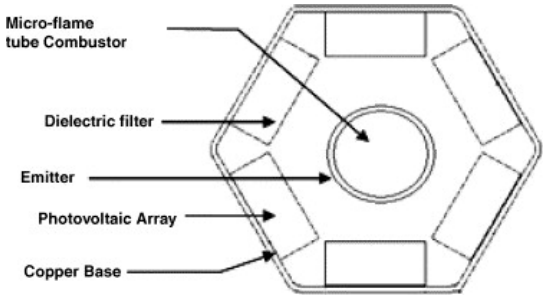

Figure 3.2: MTPV in cross-section MTPV [8]

[42]. Degradation of the combustors' structure due to heat load above the material limits can be delayed or even avoided. Nevertheless, there has also been a lot of research regarding the use of the modules together with flame combustion. There was an integrated combustor-thermoelectric micropower generator developed which combines the combustion chamber with the TE module directly. The advantage is the ability to embed components like sensors immediately during manufacturing, leading to a very compact system [9]. More recent research has been conducted on achieving a higher uniformity in temperature distribution by using perforated plates to split up the flame and thus, using flame-to-flame interaction to reach higher efficiencies [4]. This system is shown in Figures 3.3 and 3.4. It becomes visible how the TE modules are mounted in a sandwich-like manner on the outsides of the combustion chamber and cooled by a water cooler [4]. Furthermore, the effect of two-stage TE modules on the efficiency was analyzed and it turned out that the system efficiency can be enhanced by about 2% due to the improved TE module conversion efficiency, whereas the thermal efficiency of the combustor decreased [76]. Usually, the overall systems efficiency of an MTEG is at around 4%. Another important advantage of TE modules is that they do not have any wear or degradation and consequently, tend to rarely fail when they are used within their specifications [42].

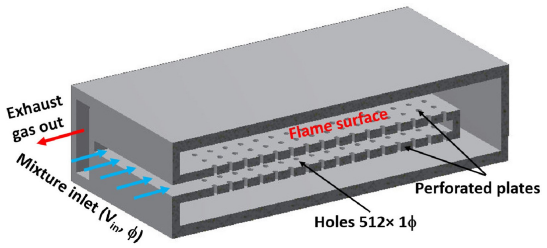

Figure 3.3: Working principle of an MTEG [4]

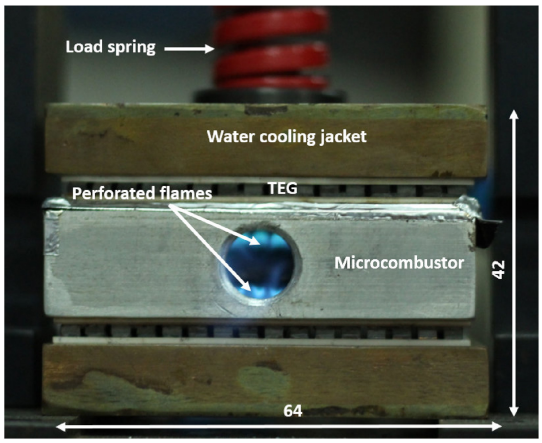

Figure 3.4: Picture of a working MTEG [4]

3.3.4. Micro Internal Combustion Engines (MICE)

MICE are systems that make use of chemical energy by moving parts. Especially this type of micropower generation system suffers from the problems occurring in microscale combustion engines. Moving parts on that scale introduce a lot of problems like leakages and friction which play a more relevant role on small scale. The most popular is the micro turbine engine from Epstein, developed at MIT as a power or thrust supply for micro-aircraft, satellites or portable power applications [18]. Micro turbine engines have a comparably low turbine inlet temperature because it is problematic to cool the turbine blades. That leads to low thermal efficiency [31]. Still, temperatures are in the range of 1600 °C with pressure ratios of 2:1 to 4:1, which limits the choice of materials [19].

Lee and Jiang proposed a design for a micro Wankel engine which has the advantage of being easy to microfabricate due to the 2D structure of its components [39]. Another concept that has been pursued in the past is the free-piston engine. A free-piston engine can be designed in single-piston, dual-piston dual-cylinder

or opposed-piston configuration, as can be seen in Figure 3.5. Either way, a crankshaft was eliminated to improve energy conversion efficiency. The explosion in the combustion chamber drives the piston and a rod attached to it. This rod is part of a linear generator that converts the energy of motion. If the system is not balanced by two combustion chambers to drive the piston back, a rebound system is necessary [28]. The combination of a free-piston engine with HCCI has been researched, where the ignition takes place in several different spots throughout the combustion chamber. In that way, the risk of flame quenching can be reduced [2]. Free-piston engines exist in all kinds of shapes.

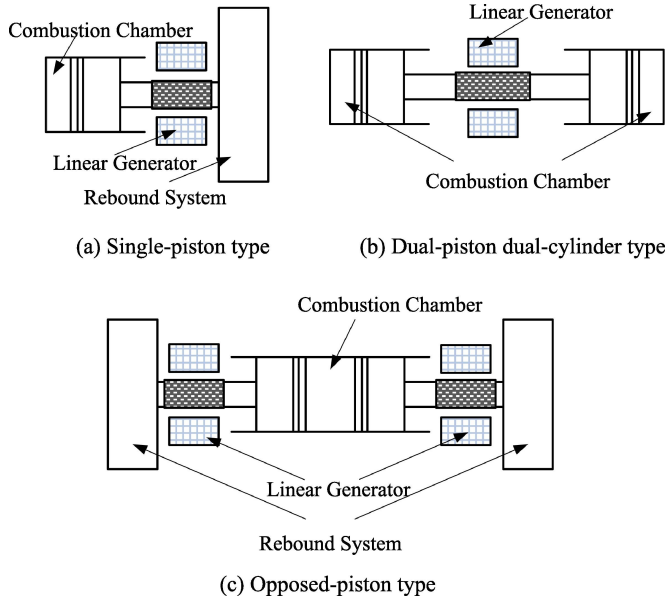

Figure 3.5: The three different configurations for balancing a free-piston engine [28]

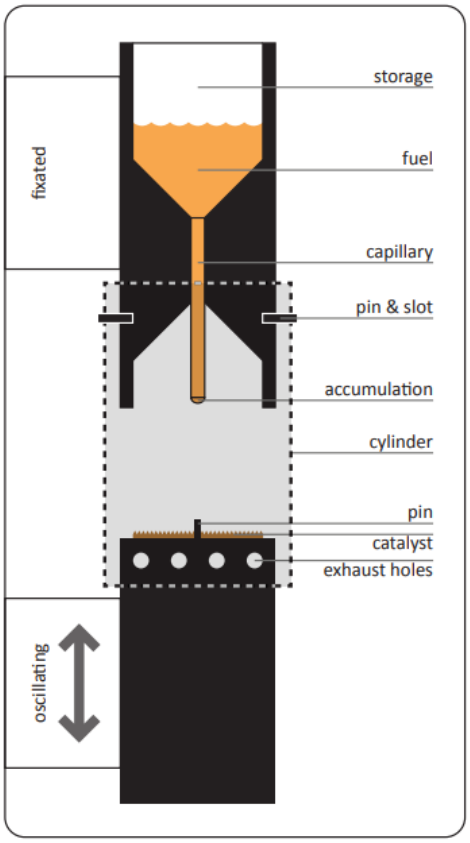

Figure 3.6: Conceptual design and working principle of the actuator built by van den Heuvel [30]

Van den Heuvel developed for example a two-stroke actuator based on catalytic decomposition to power the previously introduced Atalanta FWMAV. His designs, which served as a proof-of-concept, include passive fuel delivery and fuel storage. Despite not working properly, the experiments on the actuator gave important insights into how porous materials coated with a catalyst behave, and how fuel delivery and leakages in such a system work [30]. What the concept and its working principle look like, can be seen in Figure 3.6. Another free-piston engine is based on a compliant bellow structure. Its function and advantages are being discussed in more detail at a later point (See subsection 3.3.5).
The last internal combustion engine which shall be listed here are the Micro Internal Combustion Swing Engines (MICSE). This engine has four chambers and is characterized by its mechanical simplicity in comparison to the other MICE. The engine's cycle can be two-stroke or four-stroke, depending on the state of the opposite chambers, as shown in Figure 3.7. When two opposite chambers are in the same state, it is a four-stroke. The swingarm in the centre does not rotate fully but swings back and forth as each chamber is in a different stroke at one moment [10].
The most recently developed MICE achieve overall system efficiencies of around 10%, however, that depends on which type was chosen [71].

Another system, which does not fit into one of the above-mentioned categories is the piezoelectric energy harvesting system. Pulsed combustion in a chamber, for instance with a catalyst, causes periodic temperature deformations which are then used to generate electricity with piezoelectric material [26]. The efficiencies of

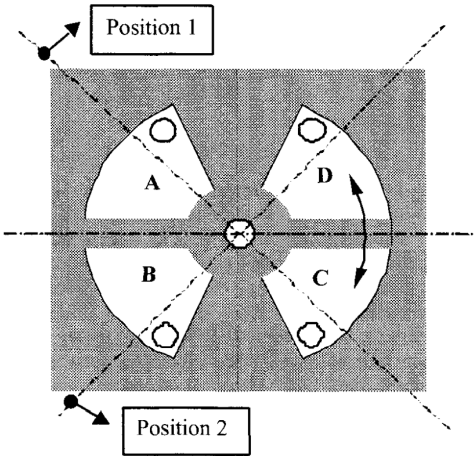

Figure 3.7: Working principle of the four chambers in a MICSE [10]

piezoelectric generators are fairly high and can reach up to 37% [35].

3.3.5. Results for Chemical Actuators

Despite a few exceptions, all actuators from recent research can be fitted into the three described categories of MTPV, MTEG, and MICE. The application defines which actuator type is chosen. For electrical applications, MTPV or MTEG are suitable but if mechanical power is needed, MICE are working best because further energy conversions are not necessary. For MTEG the trend goes towards the development of sandwich-like structures where the combustion chamber lies between two TE modules. Since TE modules work better with conduction, this is the best way of mounting them onto the chamber. Heat radiates in every direction and thus, the best method to mount thermophotovoltaic modules is in a circular pattern around the combustion chamber. Because manufacturing of curved modules is not possible with current micro-machining techniques, that has been done mostly in a hexagonal manner as can be seen in Figure 3.2. Which type of MICE is the most suitable, strongly depends on the application it is used for. Comparing the actuators in terms of overall systems efficiency is difficult because it is strongly dependent on the size of the actuator and its design. MTEG and MTPV are very similar and thus, it can be said that the latter achieves slightly higher efficiencies, whereas MICE are the most efficient micropower generators. Coming back to the FWMAV of the Atalanta project, a periodic translational motion is necessary which makes a free-piston engine the most suitable because it makes gears redundant (if the frequency of the actuator is tuned to the resonance frequency). For most mechanical-powered systems, including FWMAV, it applies that controlling the power is important. Consequently, control systems including sensors and other mission-essential electrical components require an electrical power source. All the above-mentioned MICE do not fulfil that without an additional battery which would lead back to the initial problem. Combining a MICE with either an MTPV or an MTEG could be the solution and is in that form already established in the automotive industry [50]. After analyzing the biggest reasons for the high heat losses and the low flame stability of combustion processes in the MICE a compliant combustion chamber with a catalyst based on the work from van den Heuvel was designed [30][27].

Actuator

In previous work the actuator which is described in the following was developed and marks the starting point of this project. To deal with the problem of leakage and enhance the efficiency of MICE by eliminating pressure and fuel losses, research was conducted on compliant cylinder engines. Burugupally proposed to replace conventional cylinders with super-compliant metal or composite structures, forming a flexible cavity. That eliminates leakage and friction, and thus increases the efficiency [45]. Modelling a resonant heat engine showed again, a higher heat input leads to higher efficiency of the engine because it increases its compression ratio [46]. Mous then developed a design for an actuator to power an FWMAV for a minimum of 10 minutes. Under certain conditions that he defined, the actuator would have an efficiency of 13% and would fulfil the requirements to power the FWMAV for more than 10 minutes [27]. The proposed actuator (Figure 3.8) with a compliant chamber belongs to the category of free-piston engines where the compliant structure itself is the rebound system. As soon as the pressure in the chamber increases, the chamber elongates until

the stiffness of a spring is overcome. The spring opens and releases the exhaust gas from the chamber which reduces the pressure. That causes the chamber to go back to its original length due to its own stiffness. For the energy generation of the actuator, this means that the temperature of the chamber wall is not constant but periodically changes with the fuel delivery.

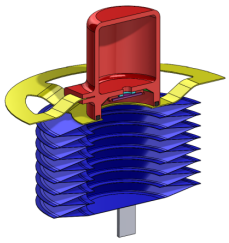

Figure 3.8: Cross-section of actuator design with compliant bellow (blue), exhaust valve (yellow), and fuel delivery with storage (red) [27]

Figure 3.9: Size comparison of the chosen compliant bellow by Guido Mous to a one euro coin [27]

For the combustion chamber an off-shelf compliant bellow with the geometrical parameters from Table 3.4 was chosen.

Design Parameter	Value
Bellow outer diameter D_0	10.1 mm
Bellow inner diameter D_i	5.08 mm
Bellow length L	4.32 mm
Maximum bellow stroke Δx	1.78 mm
O-ring sealing diameter D_s	5.46 mm
Bellow stiffness s_b	5920 N/m

Table 3.4: Geometrical parameters of the chosen compliant bellow [27]

3.4. Problem Analysis

3.4.1. Heat losses

System efficiencies of small combustion engines are, with values mostly below 10%, relatively low [61]. Here, problems specific to the presented concept of the compliant bellow are explained. That means, other problems typical to small-scale combustion like flame stability phenomena or losses due to leakage are not listed here because a compliant closed cylinder with a catalyst mostly omits them.
That makes heat loss the most dominant reason for the low efficiencies. Yang et al. calculated the heat loss ratio, so the ratio of heat loss and input chemical energy, to be about 73.6% for a cylindrical combustor of a diameter of 1 mm and 51.9% for a diameter of 11 mm [75]. It is so difficult to control the heat loss of the described systems because the surface-to-volume ratio increases with decreasing scale of the generators [22]. For rotary engines, this results in a conflicting optimization of sealing effectiveness, surface-to-volume ratio and compression ratio [24]. Even for catalytic reactions, which are area-limited and thus more feasible for small-scale combustion [1], it is favourable to reduce heat loss because increased temperatures lead to a gain in reaction speeds by a factor of 2.2 each 10 °C [3].
Figure 3.10 shows which processes of heat transfer are taking place in a flame combustion chamber which are transferrable to catalytic reactions though [75]. Yang et al. analyzed how the diameter of the cylindrical combustion chamber and the velocity of the fuel influence the heat transfer mechanisms. Among other things, they found out that the wall heat loss mostly consists of radiative heat loss whereas the heat flow into the inner surface is mostly convection. [75].

3.5. State-of-the-Art

Considering that MICE are thin-walled structures with high heat losses from the combustor wall, one could think about using TE or TPV modules not as a primary converter of heat energy into electrical energy but as

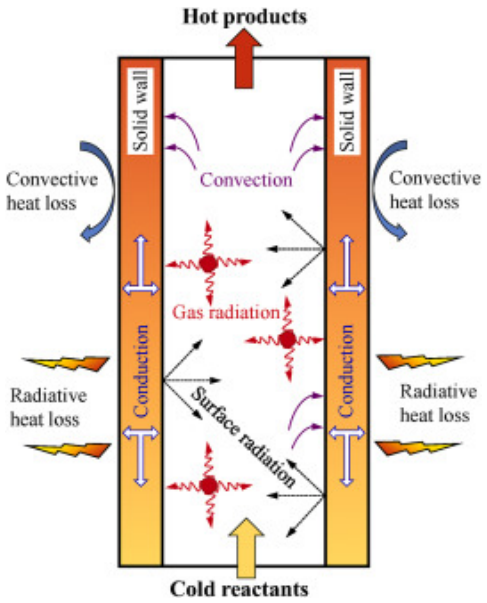

Figure 3.10: Schematic depiction of the heat flow mechanisms within a combustor [75]

a secondary, making use of the waste heat of MICE. This becomes interesting for applications where in the first place mechanical energy needs to be generated and then the overall system efficiency could be increased by generating electricity from waste heat for control systems. Jiaqiang E et al. came up with such a concept shown in Figure 3.11.

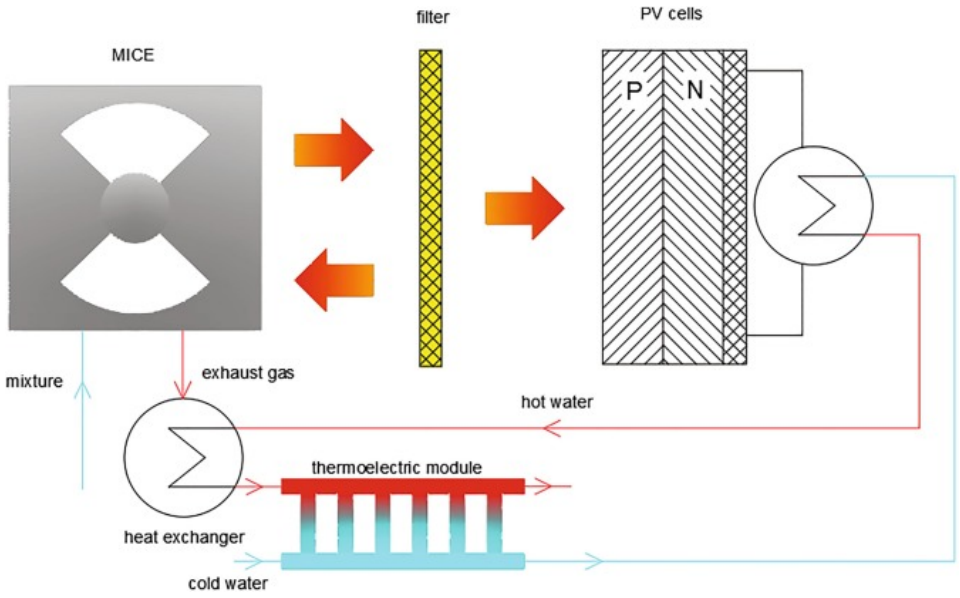

Figure 3.11: The concept of a system combining a MICE with TPV and TE [14]

3.5.1. System Breakdown and Functional Analysis

Looking at the shape of the combustion chamber it becomes clear that due to the bellow structure most heat is lost through the side walls. A system to reuse the majority of that heat would have to be thermally connected to these walls. That turns out to be rather difficult considering that the walls are moving and are of bellow shape, while the recuperation system needs to be fixed to not add moving mass to the actuator. The system around the chemical actuator can be broken down into the following components. An air gap between the combustor and the recuperation system is inevitable. The support structure holding all other components in

a place as close as possible to the heat source is considered to be part of the EGR. In that way, the structure can hold the exhaust spring in place and have channels for leading the exhaust gas from the exit at the bottom of the combustor through the recirculation. In addition to that, the components for the electricity generation can be mounted onto it and thus, be as close as possible to the heat source. In Figure 3.12 the described components of the system are depicted for a better understanding of their location and function.

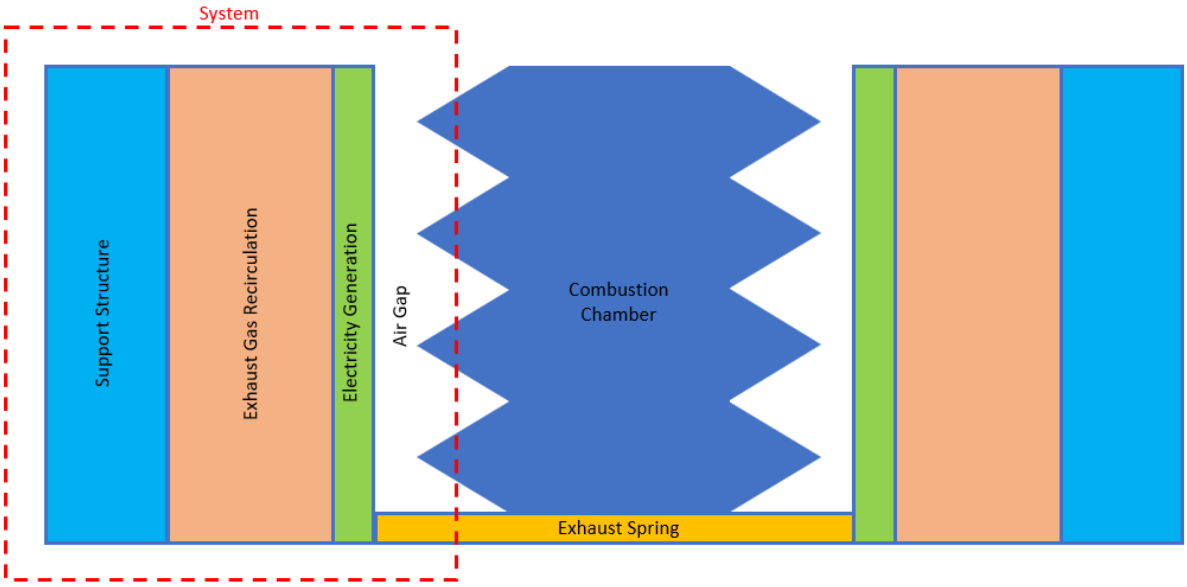

Figure 3.12: The conceptual design in a block scheme to depict its components

Component	Function
Air gap with filling	Transport heat from combustor to system
EGR	Reuse the heat from the exhaust to increase efficiency
Electrical power generation	Generate electrical power from waste energy

Table 3.5: System component and its function

It can be noted that the combustion chamber itself including the exhaust spring is considered to be similar to a grey box where the functions are known and can partially be manipulated but are generally out of scope of this research. The same goes for fuel delivery and storage where no detailed concept is known and the margin of efficiency improvement by optimizing these components is expected to be small compared to the combustion chamber [27].

3.6. Concept Generation

Air Gap with filling

In the previous sections it became clear that an air gap between the moving chamber wall and the fixed support structure is inevitable. Air has a low heat transfer coefficient and radiation, as well as convection, is becoming the dominant transfer mechanism in the gap. With regards to the modules, normally, radiation is tried to be avoided and conduction is preferred to generate a high temperature on the hot side of the module when it comes to heat transfer towards TE modules. That is why low thermal resistance and high conduction between the heat source and module are wanted. However, for changing shapes of the contact surface, like is the case for compliant combustion chambers, it could be interesting to analyze the effects of the air gap and its different fillings on power generation. The general goal for designing the air gap is to make it as small as possible. The heat transfer coefficient could be improved by the use of porous media like metallic wools with high conductivity and low stiffness so that it does not hinder the translatory movement of the bellow but at the same time transports the heat better than only air. Different materials and porosities can be tested here where the focus only lies on heat transfer and not stiffness analysis. Candidates are for example copper, aluminium or steel wools but also ESLI carbon velvets with high conductive fibres [56]. These velvets are

ultra-compliant and were developed under a NASA contract to bridge large or uneven gaps. Even surfaces that are moving relative to each other are no problem anymore since the thin fibers, fixed in an adhesive on one side, always stay in contact with both surfaces. Transfer coefficients of up to 200 W/mK are possible [49]. For TPV modules the air gap would not have as big of an impact because radiation is the preferred heat transfer mechanism.

Exhaust Gas Recirculation

From the analysis of the heat flows it is known that exhaust gas is a major reason for the high heat losses. In literature, it can be seen that many approaches have already been reviewed to make use of the energy carried by the exhaust. Often the hot products are recirculated in channels that run parallel with fuel delivery lanes. That leads to preheating of the fuel and thus to higher temperatures in the combustion chamber and higher efficiencies [40][7][13][37][38][59]. Another option for reusing the heat of the exhaust gases could be by channelling them through a second wall of the combustor to increase the temperature of the walls for the TE or TPV modules and add another insulation layer for the chamber. In that way, the modules would also have a place to be mounted on. There is a lot of research including CFD analysis and shape optimization regarding the optimization of flow patterns to increase the heat exchange and at the same time keep the flow resistance low. It should be noted that this goes beyond the scope of this work and is thus not included. For further calculations, it is assumed that there is a shape for the heat exchanger that is able to transfer the entire heat of the exhaust gas to the fuel or the TE or TPV modules. Important to keep in mind is, regarding the temperature of the exhaust gas it is not possible to reduce the exhaust gas temperature below the boiling point of water at about 100°C. Otherwise, the water of the exhaust stream condensates and starts clogging the fine exhaust channels. A third way could be no EGR at all, considering that it adds to the total weight of the structure and that the heat loss through the combustor walls could already be enough to generate sufficient heat or radiation for TE and TPV modules.

Electrical Power Generation

As explained in the previous sections, for small-scale combustion actuators the most common way of transforming the generated heat energy into electrical energy is by using TPV or TE modules. The most feasible type of module shall be chosen for the combination with the presented combustion chamber. It was already previously mentioned that the bellow structure of the combustion chamber poses problems for connecting an external structure in a way that does not disturb the heat flow. Furthermore, both types of modules need to be connected to plane surfaces which makes that even more difficult since the chamber is of cylindrical shape. To that end, it makes sense to build a support structure connecting the spring of the exhaust valve to a fixed body and also integrate channels for leading the exhaust gases through a possible recirculation and then out of the system. To minimize the air gap between the combustor wall and support structure its inner wall should have a circular cross-section while the outside wall has planar surfaces whose number is equal to build-in modules. The use of TPV cells only makes sense as long as flame combustion is used because comparably high temperatures are required for the cells to work. As soon as catalytic combustion is used, the combustion temperature lies in a range that is suitable for attaching the TE module directly to the combustor wall. To keep the support structure as thin and the modules as close to the heat source as possible it is favourable to use rather more modules, for example, 8 in an octagonal arrangement around the chamber to get closer to a circular shape. However, there is a sweet spot for the number of modules that depends on the available heat flow to generate the temperature difference over the module. That is also because the bigger the modules the more thermocouples they usually have and thus, the lower their thermal resistance.

An alternative concept for generating electricity from the original actuator is by using the previously mentioned piezoelectric harvesting systems. They would, however, not make use of the wasted energy of the original actuator but take energy from the translational oscillations of the bellow. That would change the output for powering the FWMAV or require a higher fuel input. The goal of this research though is to use waste energy that is at this moment not used by the system and consequently, reduces the efficiency of the system.

3.7. Concept Evaluation

The concepts are evaluated by first formulating design requirements based on which they are graded and later combined in a design proposal. Quantification of the requirements will only be possible to a certain degree because many parameters are unknown and are to be specified in this project.

Design Requirements Specification (DRS)

Firstly, the concept needs to be as small as possible but as big as necessary to include all features. Due to missing exact measurements for the design space, the focus lies rather on making the design as small and light as possible. The function of the compliant bellow and its interface to the FWMAV are supposed to be preserved. That includes its resonance frequency and power output which describes the input function for the thermal model of the concept that is to be developed. From the thermodynamic model of Guido Mous that he kindly provided, the exact values for different outputs regarding mass and heat flows can be extracted. One resulting requirement is that the concept for electricity generation is suitable for this specific input function (Figure 3.13). The temperatures inside the chamber reach around 350 °C at their peaks for a heat loss coefficient of 0.1 W/mK. That is so high that the temperatures drop immediately back to ambient temperature after the combustion occurs and the hot exhaust gases left the chamber.

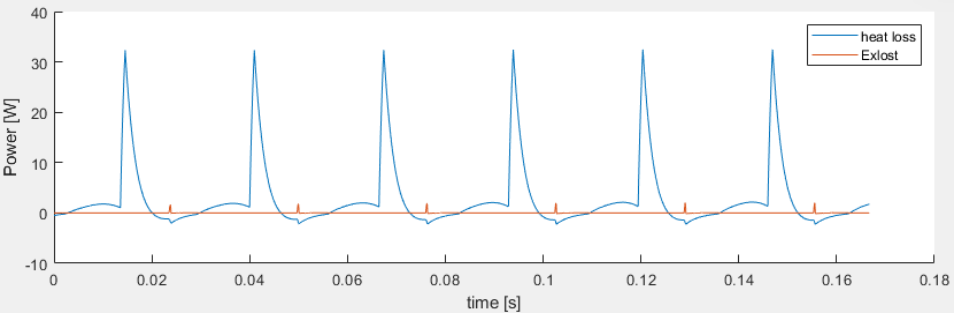

Figure 3.13: Model results from Guido Mous for heat loss through the combustor and exhaust gas respectively [27]

The concept needs to be as simple as possible while having an efficiency increase for the combustion and should consist of reliable components that lead to a relevant output of electrical power. The above leads to the following list of characteristics in which the different initial concepts are being graded. Some of them and the grading system are taken from Guido Mous [27].

- Efficiency Electricity Generation
- Efficiency Combustor
- Mass/Size
- Suitable for Power input
- Manufacturability
- Reliability
- Complexity
- Academic Relevance

3.8. Design Proposal

Based on the results from the concept evaluation an integration of the best-rated components into one system is proposed. For components like the air gap, all options keep being considered and compared at a later stage since their configurations are easily adaptable and their influence on the system performance is difficult to estimate.

3.8.1. Geometry

Figure 3.11 shows a more detailed design of the initial concept. The exact dimensions are varied in the following chapters and different combinations are evaluated. The air gap can be seen between the red-coloured compliant bellow and the light blue-coloured support structure. Between the blocks consisting of EGR, TE module, and heat sink insulating material can be placed to increase the heat flow through the structure and increase the modules' efficiency. The exact design of the support structure is not part of this project since it

Concept description	Efficiency Electricity Generation	Efficiency Combustor	Mass/Size	Suitable for Power input	Manufacturability	Reliability	Complexity	Academic Relevance
AIR GAP WITH FILLING								
Metallic wool insert • 95% porosity • 98% porosity	+ (TE) + (TPV) o (Piezo) (higher porosity = better for modules)	o	o	N.A.	++	++	++	+
ESLI Vel-Therm Gasket	++ (TE) + (TPV) o (Piezo)	+	o	N.A.	-	++	+	++
No insert	- (TE) - (TPV) + (Piezo)	++	o	N.A.	N.A.	++	++	N.A.
EGR								
Preheating fuel	+ (TE) + (TPV) + (Piezo)	++	-	N.A.	+	+	o	+
Circulation in support structure	++ (TE) ++ (TPV) + (Piezo)	+	-	N.A.	+	++	-	+
No EGR	- (TE) - (TPV) - (Piezo)	-	o	N.A.	N.A.	++	++	N.A.
ELECTRICAL POWER GENERATION								
TE module	-	+	-	++	++	++	+	+
TPV module	-	+	-	-	o	+	o	+
Piezoelectric mechanism	+	o	-	-	+	+	-	+

Table 3.6: Concept evaluation with identified characteristics. Scores: excellent (++), good(+), average (o), poor(-), very poor(–), based on [27]

only serves as a proof of concept. It should be designed as a milling part from a material with a high heat transfer coefficient like copper or aluminium. Furthermore, the structure should have mounting points for the exhaust spring and the EGR that are sealed. Channels within the structure for exhaust gas need to be aligned with the openings of the spring and the EGR. In yellow, the EGR is depicted as thin sheets of conductive copper or aluminium in which channels for the exhaust can be etched. In that way, the gas is led over the surface of the TE modules to increase their hot side temperature. In the following, different TE modules and heat sink geometries are analyzed for their feasibility for such a design. Perhaps, it turns out later that heat sinks are not necessary which would reduce the weight considerably and would clearly simplify an integration into an FWMAV or similar. To reduce contact resistances and enhance the heat transfer through the structure, surfaces of the components should be manufactured with very low roughness and very high flatness in addition to the use of some kind of thermal paste.

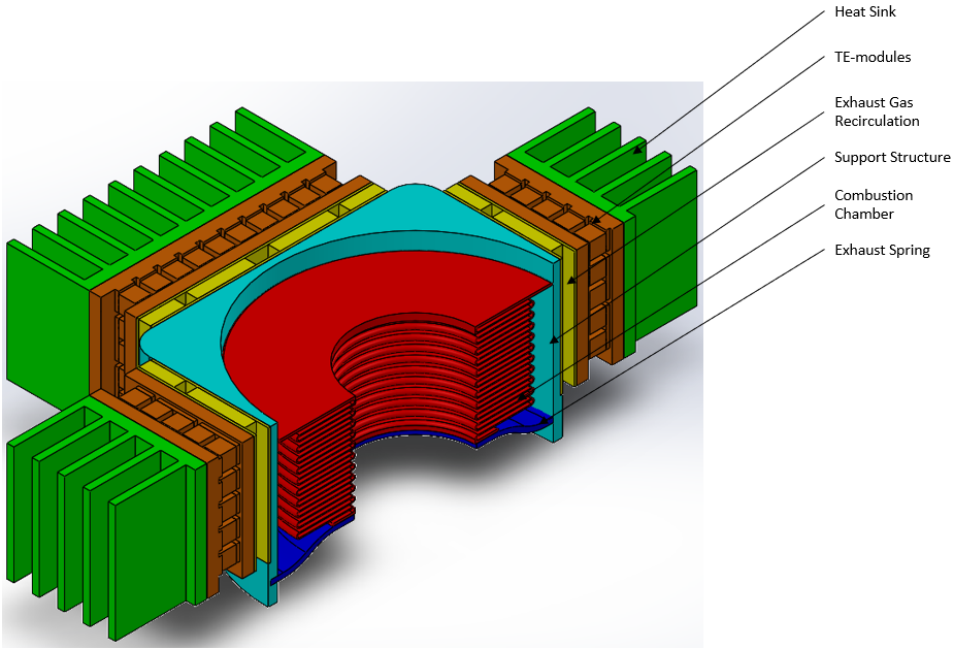

Figure 3.14: CAD model of a design proposal as the basis for a thermal model

3.8.2. Work Principle

The working principle of the concept is based on the waste heat which is assumed to flow mostly through the cylindrical walls of the combustor and the exhaust gas out of the system. Heat losses through the top and bottom can be minimized by insulating material. The flow then passes through the air gap and the EGR, where an additional heat input from the exhaust gas is led back into the system. Part of the heat energy is transformed into electrical energy when the flow creates a temperature difference over the TE module. The translational motion of the bellow is not negatively influenced by any of this. In fact, it is expected that the additional layers around the chamber decrease the heat transfer coefficient and consequently, increase the efficiency of the combustion process. Interfaces to the device are in the use case the wings of the FWMAV which need to be connected to the top part of the combustion chamber in order to oscillate with the bellow in its resonance frequency. The support structure is mounted to a non-moving part like the frame. The electrical energy generated by the TE module could be used in any electrical circuit of the device and could either be fed back into the onboard battery or power a control system. Presumably, the first option is more likely considering that the heat output of the MICE is not as stable as the output of an MTEG or MTPV.

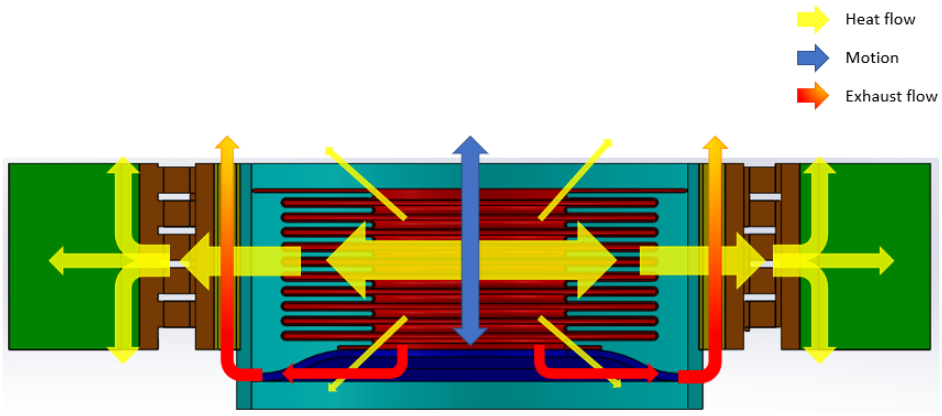

Figure 3.15: Scheme of different flows through the system

4

Steady-State Heat Resistance Model

To analyze which concepts show the best results in terms of the efficiency of the combustor and the TE modules a model of the system is being developed. If the material properties of the TE module are known, its performance crucially depends on the temperature difference across it. Thus, it makes sense to develop a heat transfer model to determine the temperatures within the system depending on the heat input generated by the combustor. In that way, many different configurations can be calculated with little effort compared to experiments or conventional software. To begin with, a steady state model is programmed in MATLAB to test each sub-model of the walls and the TE model without having transient effects. The parts are then transferred into a heat resistance-capacitance model that takes time effects into account. All parameters and geometries are chosen based on previous work conducted by Guido Mous [27] and different off-the-shelf available components. However, the results are generated in a way that they are as universally applicable as possible.

4.1. One-Dimensional Heat Transfer

At a first glance, the design concept looks structurally so non-uniform that a two- or even three-dimensional model seems obvious. However, a more detailed look shows that some valid assumptions do not change the outcome of the model too much but make it possible to stay one-dimensional and consequently simplify the model a lot. The detailed meshing of the system's components is discussed later but describing the geometry in a cylindrical coordinate system makes sense. That is due to the cylindrical formation of parts around the combustor as the central piece, even though the components attached to it are rectangular. The simplification of dealing with one dimension means heat transfer and thus, temperature differences only occur in the radial dimension while the system is uniform in phi- (angular) and z- (height) dimension. It also means, looking at the top view of the concept (Figure 4.1 left), that all heat flows through the components and only leaves the system at the heat sink. The requirement for that is ideal insulation of the room in between the components, as depicted, to achieve a low inner thermal resistance and a high thermal resistance to the outside. In reality that can be nearly accomplished by wrapping the system in highly insulating material, for example, kapton which also has the advantage of being relatively light. As a consequence, the heat flow does not get distributed across a bigger surface when moving outwards and thus, each rectangular component is modelled as a plane wall. All plane walls together add up to the total area where the heat flow passes through. In addition, smaller TE modules can be used to be able to use more modules and arrange them for example in an octagon (Figure 4.1 right). The more TE modules are used, the more the system resembles a cylindrical shape and the more admissible the assumption is.

4.2. Equations

At first, the basic equations of heat transfer are explained before the modelling of the system itself is discussed in detail. The structure of the model and underlying principles are based on "Heat and Mass Transfer" by A.F. Mills [43], all information taken from other sources is indicated as such. It should be emphasized that this work only deals with the analysis of heat transfer and does not cover thermodynamics. However, in particular, the steady-state model is entirely based on the first law of thermodynamics, also referred to as the principle of conservation of energy. The system under consideration is treated as a closed system where each component is an incompressible solid on which or by which no work is done. Some components though, for example the

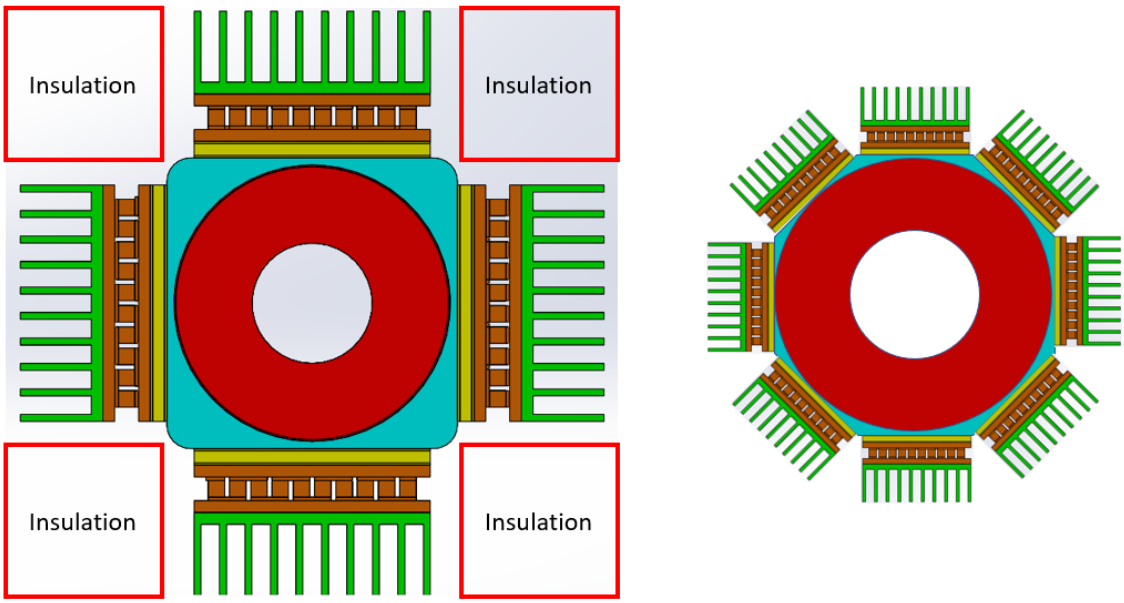

Figure 4.1: Top view of the design concept with 4 (left) and 8 (right) TE modules

combustor, have an internal heat generation. Nevertheless, the first law is equal to a heat balance in this case and mathematically written as follows,

$$\frac{dU}{dt} = \dot{Q} + \dot{Q}_v. \tag{4.1}$$

Equation 4.1 says that the change in internal energy within the system boundaries ΔU is equal to the sum of heat transferred into the system $\dot{Q}$ and heat generated within the system $\dot{Q}_v$ over a period of time. Within the system, the heat is transferred by three modes, conduction, convection and radiation, that take place as soon as there is a temperature difference. The heat always flows in the direction in which the temperature is decreasing. Since the system is in steady state at this point the heat flux through all components is assumed to be constant over time and all temperatures are only dependent on the radial coordinate. The way the temperatures are being determined throughout the system is based on the energy conservation principle which says the heat flux through the surface at r is equal to that at $r + \Delta r$ [43],

$$\dot{Q}\big|_r = \dot{Q}\big|_{r+\Delta r}. \tag{4.2}$$

For the parts where heat is generated internally, this equation changes slightly but the exact heat flows relative to their position in the system are discussed at a later point. Fourier's law for conduction is used to calculate the temperature distribution within a solid. Heat transfer is based on different phenomena like molecular collisions or vibrations. For a plane wall, it looks like equation 4.3 where the heat flux $q = \dot{Q}/A$ is proportional to the negative temperature gradient. The thermal conductivity or conductive heat transfer coefficient k $[W/mK]$ is the proportionality factor and a material constant.

$$q = -k\frac{dT}{dx}. \tag{4.3}$$

After rearranging and integrating along the thickness of the wall one gets equation 4.4 and the similarity to Ohm's law I = E/R was noticed. In this analogy, the temperature difference is seen as the voltage, the combination of L/kA is the thermal resistance, and the current is the flow of heat. By doing so, the assumption was made that the conductivity is constant over the domain which is not the case in reality. Using the analogy with Ohm's law makes it possible to simply represent heat transfer problems as thermal circuits and use the equations from electrical circuits to describe all parameters.

$$\dot{Q} = \frac{kA}{L}(T_1 - T_2). \tag{4.4}$$

Convection is the heat transfer when a fluid flows on a surface and radiation describes the heat transfer by photons. Both, Newton's law of cooling for convection and the equation describing radiation can be rearranged in a similar manner as Fourier's law. The convective heat transfer coefficient h_c $[W/m^2K]$ depends on different characteristics of the fluid flow. $h_r = 4\epsilon\sigma T_m^3$ $[W/m^2K]$, the radiation heat transfer coefficient is calculated by the multiplication of the emittances ϵ, the Stefan-Boltzmann constant σ, and T_m, the mean temperature of T_1 and T_2.

$$\dot{Q} = \bar{h_c} A(T_s - T_e), \tag{4.5}$$

$$\dot{Q}_{12} \simeq A_1 h_r (T_1 - T_2). \tag{4.6}$$

Now all three transfer mechanisms can be included in the heat resistance analogy.
As already implied, the geometry will be described in cylindrical coordinates, so Fourier's law is derived for conduction across a cylindrical shell. With $A = 2\pi rL$ equation 4.4 ends up being

$$\dot{Q} = 2\pi rL\left(-k\frac{dT}{dr}\right). \tag{4.7}$$

By assuming k is independent of temperature and rearranging the equation one ends up with a first-order ordinary differential equation for T(r).

$$\frac{\dot{Q}}{2\pi rL} = -r\frac{dT}{dr} = \text{Constant} = C_1. \tag{4.8}$$

Integrating leads to

$$\frac{dT}{dr} = -\frac{C_1}{r}, \tag{4.9}$$

$$T = -C_1 \ln(r) + C_2. \tag{4.10}$$

To determine the two constants C_1 and C_2 two boundary conditions are necessary.

$$r = r_1: \qquad T = T_1, \tag{4.11}$$

$$r = r_2: \qquad T = T_2. \tag{4.12}$$

Inserting the boundary conditions into equation 4.10 gives the two equations necessary to calculate the two unknowns C_1 and C_2.

$$T_1 = -C_1 \ln(r_1) + C_2, \tag{4.13}$$

$$T_2 = -C_1 \ln(r_2) + C_2. \tag{4.14}$$

If the second equation is subtracted from the first and then the solution reinserted into the respective equation 4.14, one is left with the constants

$$C_1 = \frac{T_1 - T_2}{\ln(r_2/r_1)}, \tag{4.15}$$

$$C_2 = T_1 + \frac{T_1 - T_2}{\ln(r_2/r_1)} \ln(r_1). \tag{4.16}$$

Substituting C_1 into equation 4.8 gives

$$\dot{Q} = \frac{2\pi kL(T_1 - T_2)}{\ln(r_1/r_2)}. \tag{4.17}$$

Using the previously discussed analogy to Ohm's law, the thermal resistance of a cylindrical shell for conduction can be calculated as follows.

$$R_{cond} = \frac{\ln(r_1/r_2)}{2\pi kL}. \tag{4.18}$$

For convection and radiation only area A needs to be replaced by the cylindrical surface.

$$R_{conv} = \frac{1}{2\pi r_1 h_c L}, \tag{4.19}$$

$$R_{rad} = \frac{1}{2\pi r_1 h_r L}. \tag{4.20}$$

Looking at Ohm's law if resistances are in series the overall resistance is calculated by the sum of all individual resistances. As soon as the current has different paths leading to the same node, the resistances are in parallel. An overall resistance can be calculated by building the sum of all conductances (K). Conductances are defined as the reciprocal of the respective resistances. That is also valid for thermal circuits. It should be noted that different heat transfer mechanisms are different paths that heat can take across a domain. That in turn means, if heat is transferred over a domain via conduction, convection and radiation at the same time, the conductances K_{cond}, K_{conv}, and K_{rad} need to be added. The reciprocal of that sum is then the overall resistance.

4.3. Components

The next step is to find a mathematical description for every component of the microactuator to build the thermal circuit and then determine the temperatures at every point in the system. In reality, contact resistances between the components can be higher than the inner resistance of the component because surface roughness and no perfect flatness bring radiation into play. Especially on small scale, these resistances become more prevalent. Nevertheless, this work does not take contact resistances into account because they are assumed to be minimized by conduction enhancements like thermal paste or precise manufacturing and because they are not expected to change the answer to the research question.

Combustion Chamber & Combustor Wall

Spatially the combustion chamber is the inside of the combustor reaching from the centerline to the compliant stainless steel wall. The bellow structure of the compliant chamber introduces variations of thicknesses in y-direction which causes the temperature to also be dependent in that direction. To keep the model one-dimensional a simplification has been made. The thickness of the combustion zone and of the air gap has been averaged in y-direction so that the corresponding heat resistance equals an average value as well. In reality, the convection coefficient of air is higher for air compared to steam which leads to lower temperatures in spots at the EGR where the bellow is the closest to the air gap and higher temperatures where it is further away. The exact temperature depending on the y-direction at these spots is not relevant. One can also assume that this difference is fairly small and also equalizes in further distance to the combustion chamber, so this assumption is admissible. Due to the catalytic reaction of the hydrogen peroxide heat is internally generated in the combustion chamber and, as can be seen in Figure 3.13, that process is time-dependent and thus, not suitable for a steady state model. To obtain an equivalent constant heat flow generated in the combustion chamber, the function for heat loss in Figure 3.13 is integrated over one second. To calculate the thermal resistance describing the combustion chamber the material needs to be known. After the reaction of the hydrogen peroxide at the bottom of the chamber, the products filling the chamber are water and oxygen. Due to the high temperature, the water is present in its gaseous form as steam. The heat transfer inside of the combustion chamber is modelled by conduction with internal heat generation which is applicable to the emission of radiation by a flame and thus, also applicable to a catalytic reaction. Therefore, the heat generation rate per unit volume $\dot{Q}_v'''$ $[W/m^3]$ is introduced. There exist two boundary conditions for the combustor saying that there is no temperature gradient at r=0 and there is a specific temperature at the outer surface of the cylinder in which heat is generated.

$$r = 0: \qquad \frac{dT}{dr} = 0, \tag{4.21}$$

$$r = r_1: \qquad T = T_1. \tag{4.22}$$

The resulting temperature distribution across the combustion chamber is described by

$$T - T_s = \frac{1}{4}\frac{\dot{Q}_v'''}{k}(r_1^2 - r^2). \tag{4.23}$$

For $r = 0$ the maximum temperature is reached which is located at the centerline of the cylinder. T_s stands for the temperature at the combustor surface and needs to be calculated before being able to obtain the temperature distribution inside the combustor. As already described earlier, the bellow shape of the combustor is ignored and that also counts for the combustor wall. For the thermal resistance, it means that it can be calculated with equation 4.18. The material for the combustor wall is stainless steel.

Air Gap

The air gap consists of the actual air gap which is as small as possible (around 0.1 mm) and the average length of the bellows (as explained in the subsection Combustion Chamber & Combustor Wall). For the air gap, different fillings of advanced porous heat transfer media are compared that have the goal to decrease the heat resistance of the air gap. That is because the bigger the resistance in a network relative to the sum of all other resistances, the higher the temperature drop over this resistance. Consequently, the aim is to choose all resistances in a way that the temperature drop across the TE module is as specified in its datasheet. If now the resistance of the air gap is much larger than the one of the TE module, most of the temperature decrease from combustor temperature to ambient temperature will happen across the air gap. Since convection and radiation are heat transfer mechanisms leading to rather high resistances compared to conduction it is favourable to find inserts that increase conduction across the air gap. It should be noted that every insert has stiffness and to increase conduction it needs to be in contact with the oscillating combustion chamber wall as well as the components on the other side of the air gap. That means, the insert will have some influence on the force developed by the combustion chamber and since that is carefully tuned, the stiffness of the insert should be as low as possible. The overall stiffness of the combustion chamber must not exceed 5000 N/m [27] and since the wool or gasket would be in parallel with the bellow, both stiffnesses would be added respectively. Regarding the airflow within the gap, it is expected that the oscillations of the chamber lead to a turbulent flow with little exchange with ambient air due to insulation and the shape of the air gap. To find out which insert fulfils all of these requirements, three promising configurations are tested in the model.

1. **Air gap without insert:** At first, the temperature distribution is analyzed for an air gap without any insert. Due to the small thickness of the air gap, not only radiation and convection but also conduction is included as a heat transfer mechanism.

2. **Air gap with metal wool inserts:** Tillack et al. analyzed the heat transfer abilities of different porous media in a comparable situation [56]. Their models predicted a higher thermal conductivity than their experiments showed and it was presumably flow bypass that caused this deviation. The exact values for the heat transfer coefficient found in the experiments are not reported. Flow bypass is not a problem for the use case of this project because within the air gap no directed flow is expected. Based on that, the model values of Tillack et al. are used in this project and taken into account as one error source for the results of this work. In Table 4.1 the transfer coefficients for different materials and porosities based on the models of Tillack et al. can be seen [56]. Porosity describes the ratio of void space and all space, so in a material with a porosity of 90% void space fills 90% of the volume of the material. The fiber diameter of the metal wools is 100 μm.

Porous Medium & Porosity	h (W/m^2K)
Copper	
98%	450
95%	1068
90%	1832
Steel	
90%	195

Table 4.1: Heat transfer coefficients for copper and steel wools of different porosities

3. **Air gap with ESLI inserts:** ESLI Vel-Therm Gaskets have already been described briefly in section 3.6. Figure 4.2 shows a microscopic image of such velvet. It is possible to not only embed one side of the velvet into an adhesive but the other side as well. The maximum bellow stroke of the considered actuator design is about 1.78 mm and it oscillates which makes it possible to design the fibers with a sufficient length to reach their maximum points respectively. Then it is possible to connect the fibers

to the bellow as well as to the support structure. In that way, the heat transfer coefficient would even be higher. In case the fibers are not on both sides embedded into an adhesive, the conductance is a

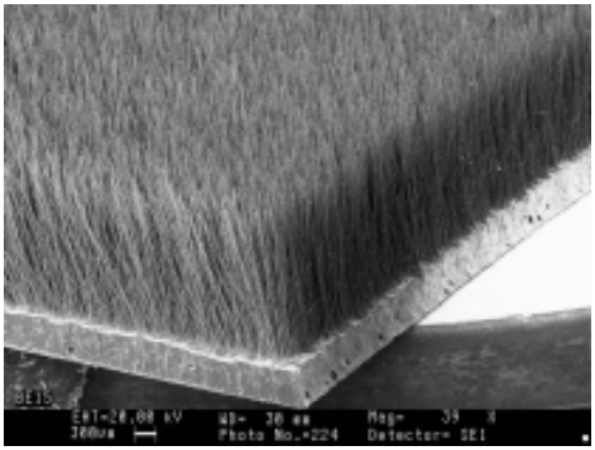

Figure 4.2: Picture of an ESLI velvet of 1 mm long carbon fibers in vinyl substrate taken by a Scanning Electron Microscope [49]

function of the pressure with which the loose end of the fibers is pressing against the wall [49]. The paper also suggests mounting the fibers already at an angle relative to the moving surface to increase conduction but due to its back-and-forth movement that would not improve in the case of a bellow. It would even risk breaking the fibers. Another option would be to apply a silicon gel with higher conductivity (0.1 W/mK) compared to air. The fibers could move in the silicon and the contact resistance would be decreased.

Exhaust Gas Recirculation

Mass flow dynamics of the exhaust gas and temperature distribution over the plate depending on the channels is not analyzed here because it is out of scope. The assumption is that a channel configuration (achieved due to optimization for example) can be found that is able to pass the gas long enough over the surface to stay only slightly above the saturation temperature. The thermodynamics of the exhaust channel could be modelled in a fairly simplified manner by setting up an energy balance over the channel including the flows from Figure 4.3. The boundaries for the balance are indicated by the dashed lines. The resulting energy balance

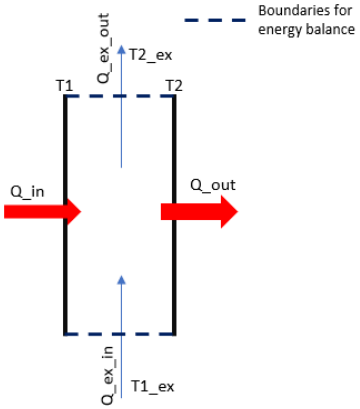

Figure 4.3: Visualization of the energy flows over the EGR channel

for this scheme is

$$Q_{in} + Q_{ex_{in}} - Q_{out} - Q_{ex_{out}} = 0. \tag{4.24}$$

The balance can be described in temperatures by introducing the average temperature of the exhaust gas $T_{ex_{avg}} = (T_{1_{ex}} + T_{2_{ex}})/2$ across the channel. The requirement for this flow balance to work is that $T_{ex_{avg}} > T_1 >$

T_2. In any other case there will not be an additional heat flow from the exhaust gas into the system but rather no flow or heat flow into the exhaust gas.

$$Q_{in} = h_c A(T_1 - T_{ex_{avg}}), \tag{4.25}$$

$$Q_{out} = h_c A(T_{ex_{avg}} - T_2), \tag{4.26}$$

$$Q_{ex_{in}} = \dot{m} c_p T_{1_{ex}}, \tag{4.27}$$

$$Q_{ex_{out}} = \dot{m} c_p T_{2_{ex}} \tag{4.28}$$

where c_p is the constant-volume specific heat [J/kg K] of the exhaust gases. Theoretically, temperature $T_{2_{ex}}$ could go as low as slightly above the saturation point for steam so that the water still leaves the channels gaseous. In that case, all the heat energy of the gas would be transferred into the system. However, for that to happen the temperature of the wall around the recirculation has to stay colder than that because otherwise, no heat flow into the system was to be present. It is assumed that the flow is laminar and fully developed with a uniform wall heat flux. Since the thickness of the channels is $0.6mm < 1/10R$ while R is the radius from the centerline to the channel, it can be considered as a plane channel. Consequently, the Nusselt number is

$$Nu_D = \frac{h_c D}{k} = 4.364. \tag{4.29}$$

To show this is a valid assumption the Reynolds number is checked. For that, the flow velocity u_b needs to be known which depends on the unknown channel diameter. Assuming the recirculation unit consists of around 32 channels, the velocity is

$$u_b = \frac{\dot{m}}{\rho \pi R^2}, \tag{4.30}$$

$$= \frac{4\dot{m}}{\rho \pi D^2}, \tag{4.31}$$

$$= \frac{4 \cdot 1.7e-6 \cdot \frac{1}{32}}{0.558\pi(0.6e-3)^2} = 0.337 \frac{m}{s}. \tag{4.32}$$

$1.7e-6 \frac{kg}{s}$ is the average mass flow calculated by Guido Mous and $0.558 \frac{kg}{m^3}$ is the density for steam at a pressure of 1 bar and a temperature of 393 K [69]. Based on the temperature-pressure relationship for saturated steam and having atmospheric pressure in the channels the lower boundary temperature is defined to be 393 K. Comparing it to the requirement for laminar flow $u_b D/\nu < 2300$ with $\nu = 0.461e-6 m^2/s$ as the kinematic velocity [60] shows that the assumption is valid.

$$Re = \frac{u_b D}{\nu} = \frac{0.337 \cdot 0.6e-3}{0.461e-6} = 438.6 < 2300. \tag{4.33}$$

From equation 4.29 and for steam $k = 0.0435$ W/m K [70] h_c becomes

$$h_c = \frac{Nu_D k}{D} = 316.39 J/kgK. \tag{4.34}$$

For further calculations it is assumed that $T_1 = T_2 = T_w$ due to the relatively high convection coefficient of steam and it later shows that this assumption is admissible. That enables the use of the equations for a single stream heat exchanger where

$$T_{2_{ex}} = T_{1_{ex}} - \epsilon \left(T_{1_{ex}} - T_w\right). \tag{4.35}$$

T_w is here the temperature of the walls and ϵ the exchanger effectiveness describing the temperature decrease of the gas in the heat exchanger divided by what is maximum possible in an infinitely long exchanger. ϵ can be calculated by

$$\epsilon = 1 - e^{-N_{tu}}, \tag{4.36}$$

where N_{tu} is the number of transfer units which is obtained by using

$$N_{tu} = n_{ch} \frac{2h_c \pi R L_c}{\frac{\dot{m}}{n_{ch}} c_p}, \tag{4.37}$$

where L_c is the length of the channel. N_{tu} is then multiplied by the number of channels n_{ch}.

TE Module

It was mentioned earlier that thermocouples generate electricity when a temperature difference from one to the other junction exists. That phenomenon is called the Seebeck effect and is made use of in a TE module where many of these thermocouples are most commonly mounted between ceramic plates. In the following, it is described how these modules can be described mathematically to include them in the steady state model. Figure 4.4 defines the variables describing the thermocouple. The basic equation describing thermoelectrics

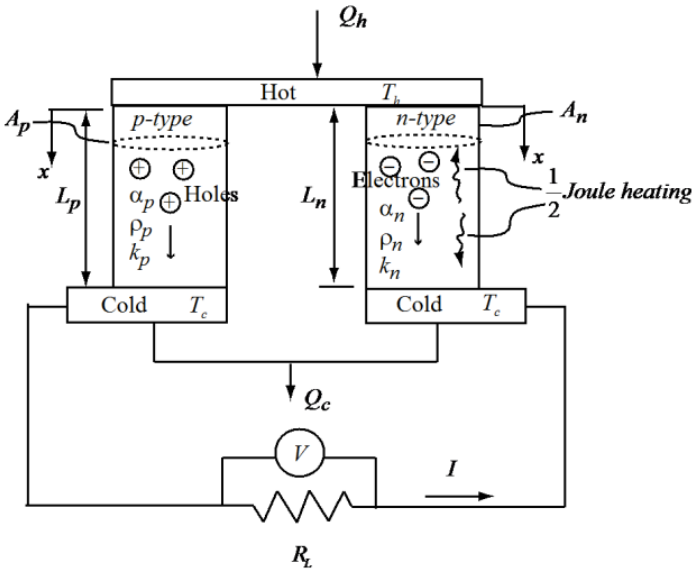

Figure 4.4: Thermocouple consisting of a p- and an n-type leg for a thermoelectric generator [32]

is the following and shows that thermoelectrics and thermal conduction are independent of one another.

$$\boldsymbol{q} = \alpha T \boldsymbol{j} - k \boldsymbol{\nabla} T. \tag{4.38}$$

α is the Seebeck coefficient. The general heat diffusion equation for steady state is defined as

$$-\boldsymbol{\nabla} \cdot \boldsymbol{q} + \dot{q} = 0 \tag{4.39}$$

with $\dot{q}$ as

$$\dot{q} = \boldsymbol{E} \cdot \boldsymbol{j} = j^2 \rho + \boldsymbol{j} \cdot \alpha \boldsymbol{\nabla} T. \tag{4.40}$$

If equations 4.38 and 4.40 are inserted into 4.39, the result is the second basic equation describing thermoelectric phenomena,

$$\boldsymbol{\nabla} \cdot (k \boldsymbol{\nabla} T) + j^2 \rho - \tau \boldsymbol{j} \cdot \boldsymbol{\nabla} T = 0 \tag{4.41}$$

with $\tau = T \frac{d\alpha}{dT}$ as the Thomson coefficient. Equation 4.41 combines the conductivity (first term), the effects of Joule heating (second term) which describes the heating of a material when an electrical current passes through and the Thomson effect (last term). The latter is based on the Seebeck coefficient not being constant over the material domain which then causes temperature differences that in turn again drive a current. Equation 4.41 can be simplified by neglecting electrical and thermal contact resistances as well as radiation and convection at the surfaces, considering the Seebeck coefficient to be independent of temperature. If it is then applied to a thermocouple (Figure 4.4) it can be written as

$$\frac{d}{dx}\left(kA\frac{dT}{dx}\right) + \frac{I^2 \rho}{A} = 0. \tag{4.42}$$

After different rearrangements and substitutions one ends up with the following set of equations describing the power and current output, temperature difference and efficiency of TE modules in a simplified manner.

$\dot{Q}_h$, the heat energy absorbed at the hot side of the TE module and $\dot{Q}_c$, the heat flow leaving the cold side are

$$\dot{Q}_h = n\left[\alpha T_h I - \frac{1}{2}I^2 R + K(T_h - T_c)\right], \tag{4.43}$$

$$\dot{Q}_c = n\left[\alpha T_c I + \frac{1}{2}I^2 R + K(T_h - T_c)\right] \tag{4.44}$$

where n is the number of thermocouples, R is the electrical resistance and K is the thermal conductance. They are defined as

$$\alpha = \alpha_p - \alpha_n, \tag{4.45}$$

$$R = \frac{\rho_p L_p}{A_p} + \frac{\rho_n L_n}{A_n}, \tag{4.46}$$

$$K = \frac{k_p A_p}{L_p} + \frac{k_n A_n}{L_n}. \tag{4.47}$$

According to the first law of thermodynamics the difference in the heat flows is the electrical power $\dot{W}_n = \dot{Q}_h - \dot{Q}_c$ generated by the module.

$$\dot{W}_n = n\left[\alpha I (T_h - T_c) - I^2 R\right]. \tag{4.48}$$

Introducing a load resistance R_L the performance parameters of the TE module can be written in the following way.

$$I = \frac{\alpha (T_h - T_c)}{R_L + R}, \tag{4.49}$$

$$V_n = n\left(\alpha (T_h - T_c) - I R_{el}\right), \tag{4.50}$$

$$\dot{W}_n = \frac{n\alpha^2 (T_h - T_c)^2}{R} \frac{\frac{R_L}{R}}{\left(1 + \frac{R_L}{R}\right)^2}. \tag{4.51}$$

The conversion efficiency of the module [15] can then be calculated by

$$\eta_{th} = \frac{\dot{W}_n}{\dot{Q}_h} = \frac{n R_L \Delta T \alpha^2}{K (nR + R_L)^2 + n (R_L T_h + nRT) \alpha^2}. \tag{4.52}$$

The maximum current can be achieved by setting $R_L = 0$ and thus, creating a short circuit. For obtaining the maximum voltage, I = 0 needs to be achieved by creating an open circuit. To maximize the power output and consequently, also achieve the maximum power efficiency η_{max} the ratio between the resistances needs to be $\frac{R_L}{R} = 1$. This ratio needs to be $\frac{R_L}{R} = \sqrt{1 + Z\bar{T}}$ for achieving the maximum conversion efficiency. $\bar{T} = \frac{T_h + T_c}{2}$ is the average temperature across the TE module and $Z = \frac{\alpha^2}{\rho k}$ the dimensionless figure of merit.
The problem with these ideal equations is the assumptions made in the beginning. Especially for Micro Electro Mechanical Systems (MEMS) neglecting contact resistances or heat leakage can lead to inaccurate models and wrong predictions about efficiency or output power [68]. There exist different approaches to obtaining equations that return a good approximation of the performance of a TE module. Wu et al. went over solving the non-simplified equations and ended up with a solution consisting of three equations that describe T_h, I and T_c. They compared the output for different coefficients to a commercial module and analyzed the effects of turning off the Thomson effect or contact resistances [68]. Another concept that was pursued by different people is to use the simplified equations presented above and to develop effective material properties for the module. These can then be inserted into the ideal equations to take certain effects into account [63].

$$\rho^* = \frac{4(A/L)\dot{W}_{max}}{n I_{max}^2}, \tag{4.53}$$

$$\alpha^* = \frac{4\dot{W}_{max}}{n I_{max} (T_h - T_c)}, \tag{4.54}$$

$$Z^* = \frac{1}{\bar{T}}\left[\left(\frac{1 + \frac{\eta_{max}}{\eta_c}\frac{T_c}{T_h}}{1 - \frac{\eta_{max}}{\eta_c}}\right)^2 - 1\right], \tag{4.55}$$

$$k^* = \frac{{\alpha^*}^2}{\rho^* Z^*}. \tag{4.56}$$

That the effective properties are based on the maximum parameters of the module, as can be seen in equation 4.56, and not on the thermoelectric properties itself is an important advantage. That is because, on the contrary to the latter, the maximum parameters are mostly provided by the manufacturers.

Heat Sink

The heat transfer from the cold side of the TE module to the air happens mostly via convection. Since the convective heat transfer coefficient for air is relatively small the consequence could be a high resistance between the module and air. As mentioned earlier, the higher this resistance is relative to the other resistances the higher the temperature drop is. To be able to control this resistance a heat sink is added to the model whose geometrical and material properties can be used to optimize the heat transfer to the surroundings. The new heat transfer coefficient of the heat sink is calculated by equations for extended surfaces like fins. It was decided to go with a straight rectangular fin. The thermal resistance of a finned surface is

$$R = \frac{1}{h_c A \eta_i}. \tag{4.57}$$

The necessary parameters for using this are obtained by the following equations. The exact temperature distribution in the heat sink is not of interest so the heat sink is represented by a single resistance with a node on the hot side and a node on the cold side. η_i as the total surface efficiency can be calculated by

$$A\eta_i = \left(A - A_f\right) + \eta_f A_f. \tag{4.58}$$

A is the total surface area available for heat transfer to the ambient while A_f is the surface area only of the fins. η_f is the efficiency of the fins which can be calculated for rectangular fins by

$$\eta_f = \frac{1}{\beta L} tanh\beta L, \tag{4.59}$$

where L is the length of the fins and β can be calculated by

$$\beta = \sqrt{\frac{h_c}{kt}}. \tag{4.60}$$

h_c is the convective heat transfer coefficient (in this case air) and k is the conductive heat transfer coefficient of the material of the heat sink. t is the thickness of one fin. In Figure 4.5 the mentioned areas are shown for

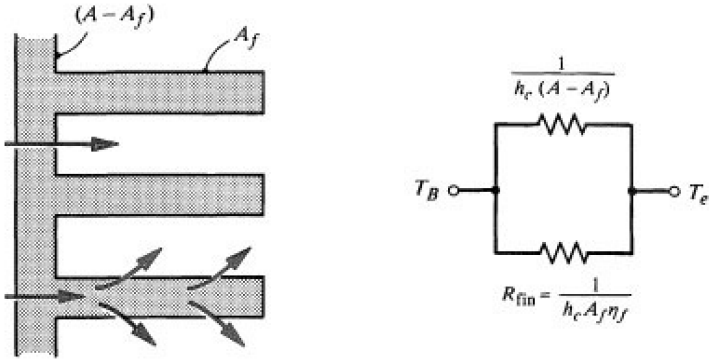

Figure 4.5: Depiction of the areas and heat flows needed to calculate the heat resistance of the heat sink [43]

better understanding.
Zhou et al. analyzed how the design of the heat sink affects the performance of a thermoelectric generator from the two sides of having either a fixed heat sink and then optimizing the resistance of the TE module or the other way around with a fixed TE module. For the first case, the resistance of the module should be matched to the resistance of the heat sink. The second one is more interesting for this work since different but in itself, fully defined modules are being used and the heat sink can be adapted to it. The results show that the heat sink resistance should be as small as possible and is only limited by the optimal temperature drop over the TE module. That means the resistance needs to be minimized until the temperature drop over the module is equal to the maximum specified drop by the manufacturer [77].

Materials and Coefficients

After seeing the theory behind the model described in the previous sections it becomes clear that material choices need to be made from which different coefficients, necessary for the model, result. The used coefficients are listed in section A.1 of the appendix. Guido Mous calculations show that temperatures of around 600 K are reached in the combustion chamber [27], so most temperature-dependent coefficients are implemented in a range from 200 K to 800 K to cover the entire spectrum of possible temperatures. The buffer is added because of the numerical nature of the model which could lead to higher temperatures in iterations during the convergence process. Higher temperatures are not considered since they are unrealistic in the configuration due to the melting points of materials like aluminium. The values in between the given temperature-coefficient pairs are obtained by linear interpolation. It is assumed that the coefficients are constant over the entire domain of the components respectively. Table 4.2 lists the used materials for the components.

Component	Material	
Combustor	Water (Steam)	The products of the catalytic reaction are water and oxygen at a high temperature. The water is present as steam.
Combustor wall	Stainless Steel	Depends on the bellow. Here the one chosen by Guido Mous was taken [27].
Air gap	ESLI, copper, steel & air	The different configurations were described in section 4.3.
EGR	Aluminium & exhaust gas (steam)	The steam is channelled between two thin aluminium plates which are conductive, available and easy to manufacture.
TE module	N-type & p-type beryllium telluride	Given by manufacturer.
Heat sink	Aluminium	Heat sinks are available in a big variety of sizes and shapes in aluminium and are easy to manufacture in case of customization.

Table 4.2: The selection of materials for the individual components

Heat Flows

To calculate the temperatures at the nodes the resistances and the heat flows through each element need to be known, so Fourier's law of conduction, Newton's law of cooling and the similar equation for radiation can be applied. Due to an additional heat inflow from the EGR and an outflow from the TE module, the heat flow through the system is not constant. In Figure 4.6 the different heat flows from the centerline of the cylindrical combustor to the ambient are visualized. The meshing is discussed in more detail in section 4.4 and is for now

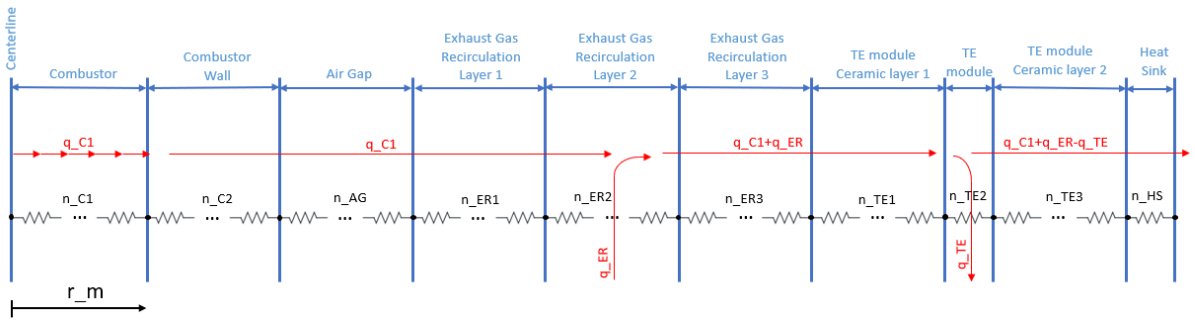

Figure 4.6: Flowchart showing the different heat flows through the components (distances do not represent actual dimensions)

considered as given. It can be seen that in the combustor heat is generated by the catalytic reaction which then flows outwards in the direction of the environment due to its lower temperatures. Until the EGR, the heat flow stays constantly at the power generated by the combustor. After the EGR, an additional heat flow is added to the heat flow from the combustor and the sum of both is used to calculate the temperatures in between the recirculation and the TE modules. As can be seen in the equations for TE modules there is heat energy transformed into electrical energy, so the heat flow after the modules passes the ceramic wall of the module and the heat sink is decreased by that amount. It is obvious that the heat flow is not constant over the

domain which complicates the temperature calculation. In most examples that make use of the equations for the TE modules, some temperature on the hot side of the module is known from measurements. The thermal unknowns for which the system of equations needs to be solved are thus, normally $\dot{Q}_h$ and $\dot{Q}_c$. Here, however, only the input heat flow generated by the combustor is known and the maximum temperature in the system also depends on the heat flow on the cold side of the module. Consequently, the thermal unknowns are now $\dot{Q}_c$, T_h and T_c, so another equation is needed to solve the system. This equation relates the cold side heat flow $\dot{Q}_c$ to the temperature T_c via the ambient temperature T_{amb} where R_c is the sum of all resistances on the cold side of the module.

$$T_c = T_{amb} + \dot{Q}_c R_c. \tag{4.61}$$

Regarding the EGR it makes sense to check the temperature distribution first before implementing it, considering that it only adds heat to the system if the gas is hotter than the channel walls. Therefore, the modules are mounted directly onto the support structure (in Figure 4.6 *EGR Layer 1*).

4.4. Model Workflow

After discussing the governing equations and the modelling of each component in the previous sections 4.2 and 4.3 now the general function of the model is explained. Figure 4.7 shows a flowchart for the numerical model depicting how the temperatures in the system are determined.

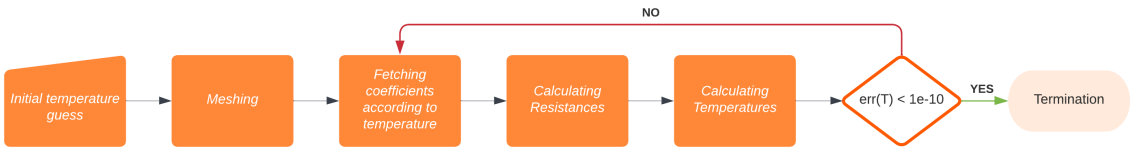

Figure 4.7: Flowchart showing how the temperatures in the system are calculated

Initial Guess & Meshing

The first step is guessing an initial temperature for each component which is somewhat reasonable and lies within the temperature range for which coefficients are existing. After that, each component is divided into a predetermined number of elements. Which number of elements leads to convergence is analyzed in a mesh sensitivity analysis at a later stage. For the TE module and heat sink, a number of elements above one is not allowed due to the chosen governing equations.

Fetching Coefficients & Calculating Resistances

When the domain is meshed and the initial temperature guess is applied to each node between the elements, the respective coefficients are chosen depending on the temperature and material of the element. As mentioned earlier, for temperatures in between the defined points the coefficients are linearly interpolated. For the interpolation, the function ScaleTime from Jan Simon was used to accelerate the process [34]. Based on the equations discussed before, the resistances of each element are determined.

Calculating new Temperatures & Error for Termination

The system of equations is divided into two subsystems where one calculates the temperatures and heat flow associated with the EGR while the other does that for the TE modules. Since the latter requires knowledge about q_{ER} (Figure 4.7) the equations for the EGR listed below are solved first.

$$q_{ER} = q_{C1} + \dot{m} c_p (T_{1_{ex}} - T_{2_{ex}}), \tag{4.62}$$

$$T_s = T_w + q_{C1} \sum R, \tag{4.63}$$

$$T_{2_{ex}} = T_{1_{ex}} - \left(T_{1_{ex}} - T_w\right)\left(1 - e^{-N_{tu}}\right). \tag{4.64}$$

T_s is here, as before, the temperature at the combustor wall and T_w is the temperature at the EGR wall. $T_{1_{ex}}$ and $T_{2_{ex}}$ are the temperatures of the exhaust gas at the entrance and exit of the channel respectively. $\sum R$ is the sum of resistances between T_s and T_w. The variables for which these equations are solved are q_{ER},

$T_{2_{ex}}$ and T_s where the solution of the temperatures has to lay between the limits of ambient temperature and 800K. The now-determined values from the first subsystem of equations are inserted into the next subsystem containing the following equations.

$$\dot{Q}_h = n\left[\alpha T_h I - \frac{1}{2}I^2 R + K(T_h - T_c)\right], \tag{4.65}$$

$$\dot{Q}_c = n\left[\alpha T_c I + \frac{1}{2}I^2 R + K(T_h - T_c)\right], \tag{4.66}$$

$$I = \frac{\alpha(T_h - T_c)}{R_L + R}, \tag{4.67}$$

$$V_n = n(\alpha(T_h - T_c) - IR_{el}), \tag{4.68}$$

$$\dot{W}_n = \frac{n\alpha^2(T_h - T_c)^2}{R} \frac{\frac{R_L}{R}}{\left(1 + \frac{R_L}{R}\right)^2}, \tag{4.69}$$

$$\eta_{th} = \frac{\dot{W}_n}{\dot{Q}_h} = \frac{nR_L(T_h - T_c)\alpha^2}{K(nR + R_L)^2 + n(R_L T_h + nRT)\alpha^2}, \tag{4.70}$$

$$T_c = T_{amb} + \dot{Q}_c R_c, \tag{4.71}$$

$$T_{2_{ex}} = T_h + \dot{Q}_h R_h. \tag{4.72}$$

$\dot{Q}_h$ as the heat flowing into the modules is equal to q_{ER}. The way the listed equations are set up ensures that the first law of thermodynamics is not violated. Both systems together contain in total 9 equations which are used to determine the following 9 unknowns. Based on the now-known temperatures at the crucial nodes

$$T_h \quad T_{2_{ex}} \quad T_c \quad T_s \quad I \quad \dot{Q}_c \quad q_{ER} \quad \dot{W}_n \quad V_n \quad \eta_{th}$$

of the system, Fourier's law can now be applied to determine the temperatures at the nodes in between by using the corresponding heat flows. The temperature distribution in the combustion chamber is calculated by using the equations described in section 4.3. After every iteration, the newly calculated temperature vector is compared to the one of the previous iteration until the error between them reaches a value smaller than 1e-10. The error is calculated for every node individually by

$$err(T) = \left|\frac{T - T_{prev}}{T_{prev}}\right| < 1e-10. \tag{4.73}$$

4.5. Verification

The proposed model can be validated in multiple ways like experimental validation or combining this with building the same model in commercial software. Due to time restrictions and the fact that the results can be fairly easily checked by reasoning, it was decided to only verify parts of the model. Nevertheless, considering the simplifications and assumptions made, experiments should be conducted to determine the accuracy of the model and not only its correctness. Included in the verification are a simplified version of the model's workflow and the validation of the equations for the thermoelectric modules. The calculations of the resistances have their origin in basic equations and material coefficients that have been collected from trustworthy sources, so their validation was omitted.

Workflow of the Model

Figure 4.8 shows initial model results for heat flow, temperature, and resistance over the radius to show the validity of the model. The red lines in the top left depict the boundaries between the components. Comparing with the graph of the resistance over radius shows that the shape of the temperature graph makes sense since the temperature drop at components with little resistance is small while the drop at the TE legs or the heat sink is bigger. Also, the ratio between the drop at the module and the drop at the heat sink being nearly twice as much at the heat sink is reasonable and testing with different resistances for both components shows the expected change in temperature distribution. Zooming into the area of the combustor, the temperature shows the exponential graph fitting equation 4.23. All layers until the air gap are modelled in cylindrical walls, so the resistances decrease logarithmically while the outer layers modelled by plane walls in cylindrical formation have linear resistance decrease. In addition, the heat flow through the system also does not leave a

reason to believe that the results are not correct. The value reaches the total heat set free by the combustor at its outer surface, increases at the EGR, and then drops by a small amount of Watts at the TE module. During

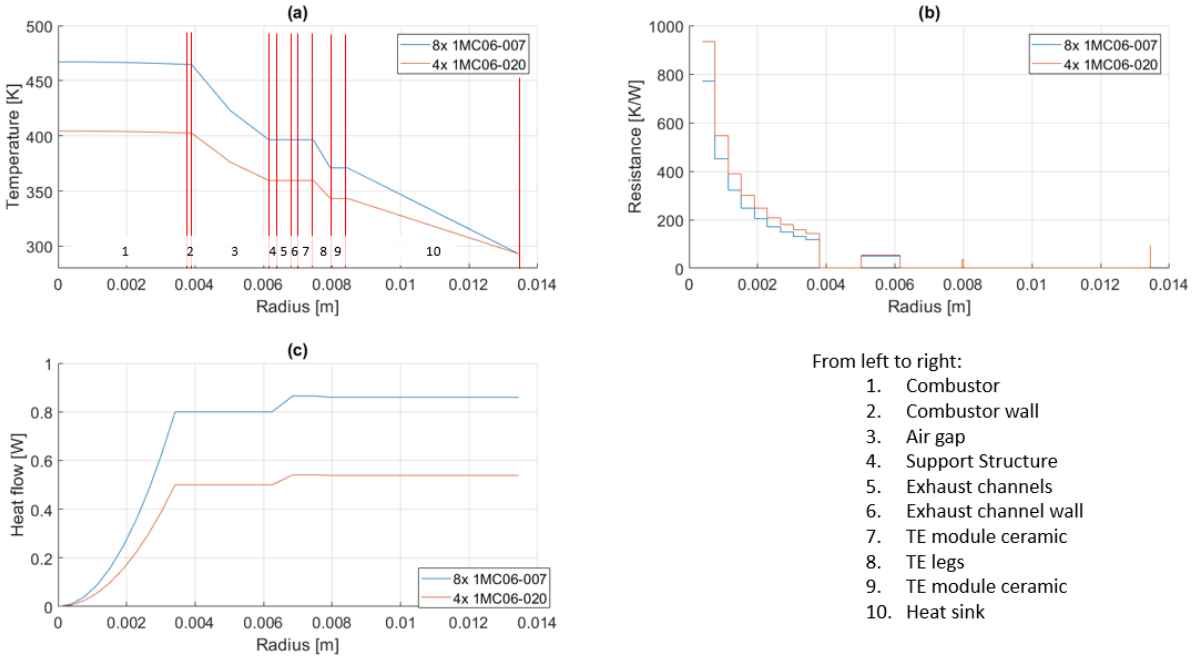

Figure 4.8: Initial results for Verification ($q_{C1} = 0.8W$ with EGR)

the presentation of the results the model is further verified by analyzing various dependencies and inputs.

Equations for the TE Module

The results of the ideal equations for TE modules applied to an exhaust waste heat recovery system were compared to results from lecture material [32]. For the given values

$$\alpha_p = -\alpha_n = 168\mu V/K \qquad \rho_p = \rho_n = 1.56e-3\Omega cm$$
$$k_p = k_n = 1.18e-2W/cmK \qquad A_p = A_n = 12mm^2$$
$$T_h = 503K \qquad T_c = 323K$$
$$L_p = L_n = 4.6mm \qquad N = 98 \text{ couples}$$

the results match the given ones listed below.

Results in Literature	Reproduced Results
$Z = 1.533e-3K^{-1}$	$Z = 1.5e-3K^{-1}$
$Z\bar{T} = 0.633$	$Z\bar{T} = 0.6335$
$I = 2.528A$	$I = 2.5284$
$R = 0.01\Omega$	$R = 0.0120$
$V_n = 2.964V$	$V_n = 2.9635$
$\dot{W}_n = 7.493W$	$\dot{W}_n = 7.4930W$
$\eta_{mp} = 0.051$	$\eta_{mp} = 0.0511$

The results for the effective material properties were compared to the manufacturer's data sheets of three different TE modules. Graphs were generated showing the relationship between the output power and the load voltage over the hot side temperature as well as the efficiency over the load resistance and the output voltage with output power over output current [32]. The exact values could be reproduced and their graphs can be seen in Figures 4.9 to 4.12. Figure 4.13 shows the same results from literature compared to experiments [32].

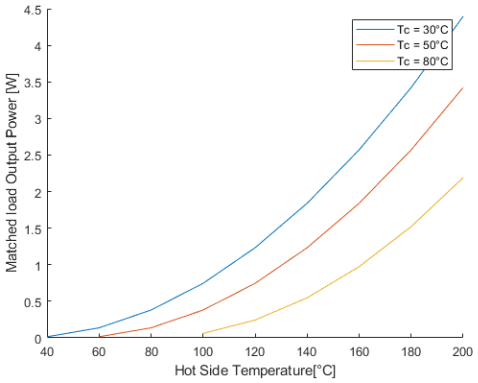

Figure 4.9: Power over T_h for TGM127

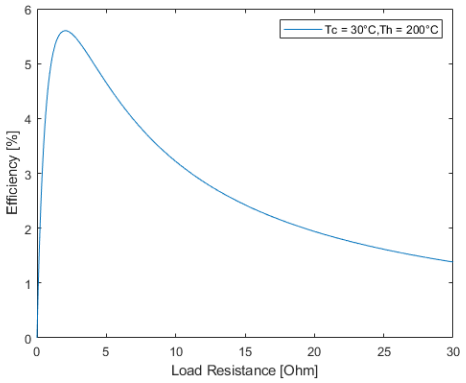

Figure 4.11: Efficiency over R_L for TGM127

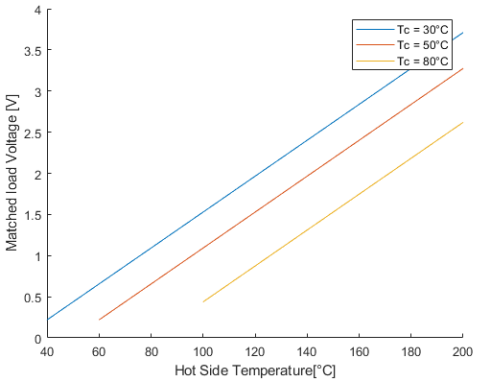

Figure 4.10: Voltage over T_h for TGM127

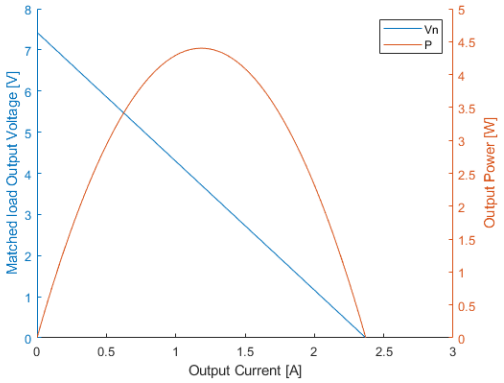

Figure 4.12: Voltage & power over I for TGM127

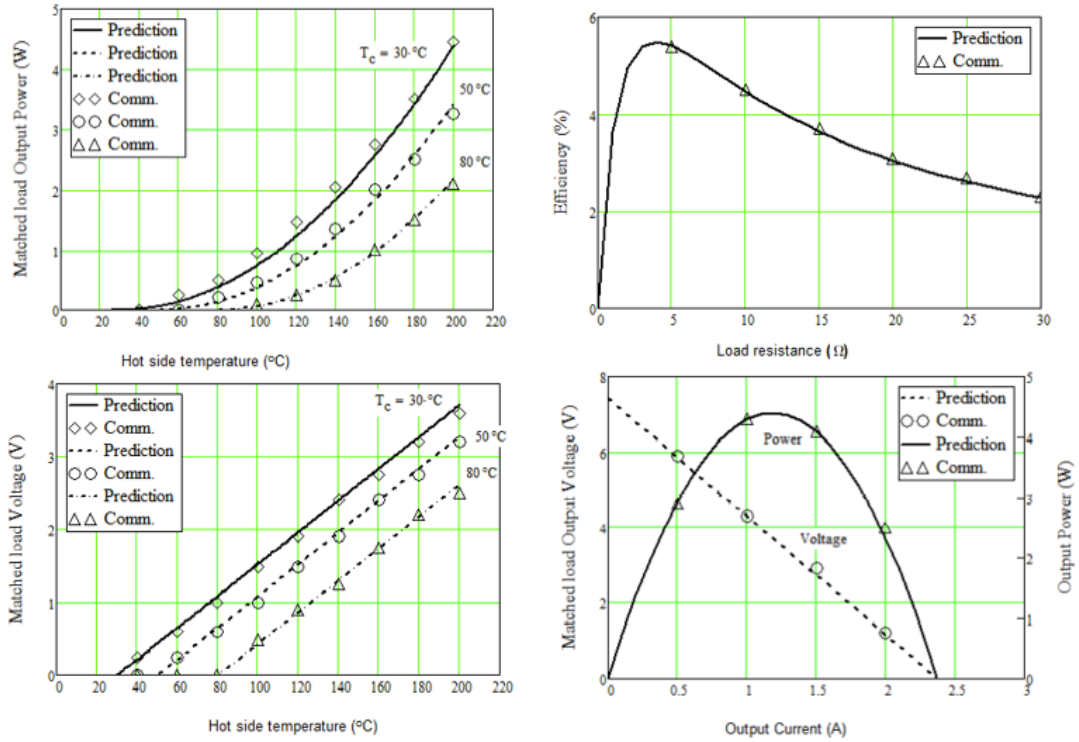

Figure 4.13: Results from literature showing the correctness of the results in Figure 4.9 to Figure 4.12 [32]

4.6. Results

As already previously mentioned, at first the system is modelled without using EGR to check whether there is a temperature difference between the exhaust gas temperature and the wall temperature big enough to transfer additional heat from the gas into the walls. To this end, the temperature distribution along the radial coordinate is evaluated for different configurations. As a start, the temperatures for the calculated heat input and no porous media in the air gap are determined. This combination of input and configuration leads to no solution since temperatures of well over 1300 K are calculated and no coefficients are defined in that temperature range. These temperatures are considered unrealistic due to exceeding the limits of some of the used materials so the heat flow is reduced to a point where a solution is possible. The upper temperature limit chosen for this case is 800K and the lower boundary is defined by the characteristics of steam. In the temperature range the actuator is operating in, both saturated and superheated steam could be present. While saturated steam has a defined temperature-pressure curve superheated steam develops when saturated steam is heated even further. For heat exchangers, saturated steam is the more common choice since more heat can be transferred from the steam to the surface by partial condensation in the form of a film or droplets. This is, however, not wanted for the considered application because the condensate could inhibit the catalytic reaction and clog the fine pipes. To avoid that it was decided to keep the steam above its saturation temperature. In the chamber where pressures of up to 4.5 bar were calculated by Guido Mous [27] the minimum temperature is thus 155 °C (429 K) and for the EGR at 1 bar is 120 °C (393 K). As described earlier, it is difficult to obtain hydrogen peroxide with a high purity and superheated steam is known for causing accelerated fouling [41]. The impurities can lead to material deposits on the channel walls and together with the high temperature of the steam lead to corrosion. How severe that effect is, should be part of further research. For air as the medium in the gap, a feasible heat flow of 0.065 W is leading to the results depicted in Figure 4.14. Higher heat in-

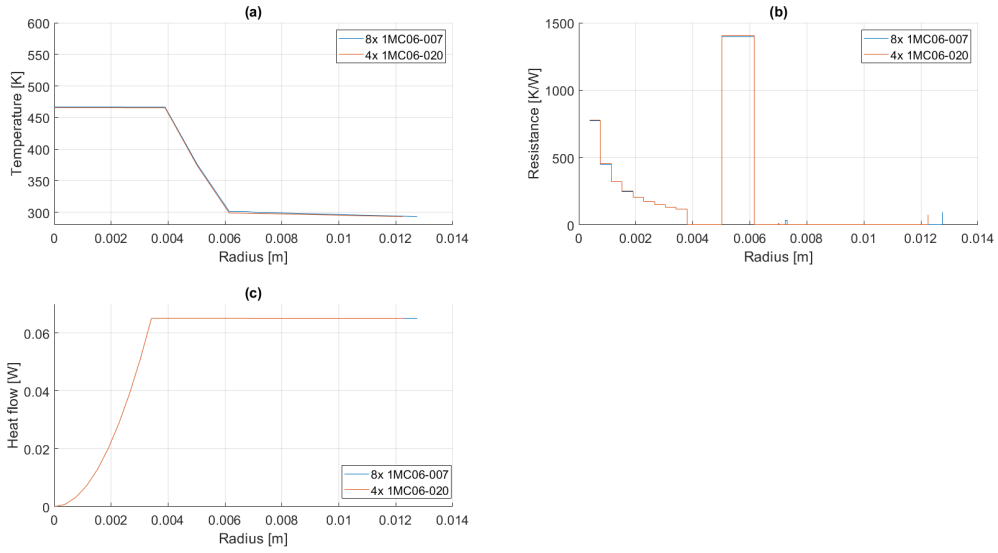

Figure 4.14: Results for air in the air gap and heat flow of 0.065 W

puts were despite the relatively low maximum temperature not possible because the model took more than 2000 iterations to converge to the result. The solution often jumped outside the defined range of coefficients during the process. The results for the two TE modules have been compared and no major difference can be noted between the graphs. Only the heat resistance of the 8 smaller modules is comparatively higher. However, that makes no difference for the occurring temperature distribution or heat flow since the temperature difference across the modules is so low that no electrical power output can be seen. The heat resistance of the air gap is so much higher than the rest of the system that the temperature drops solely over the gap. Here it becomes especially clear that it makes sense to reduce the resistance of the air gap, for instance by porous media, and include an EGR to increase the temperature after the gap. At the large temperature drop at the air gap, it can be seen that modelling the components at the outer layers of the system as plane walls has a negligible effect on the temperature graph. Even for such a large temperature difference the logarithmic function is approximately linear. If for the same configuration of 8 TE modules different materials in the air

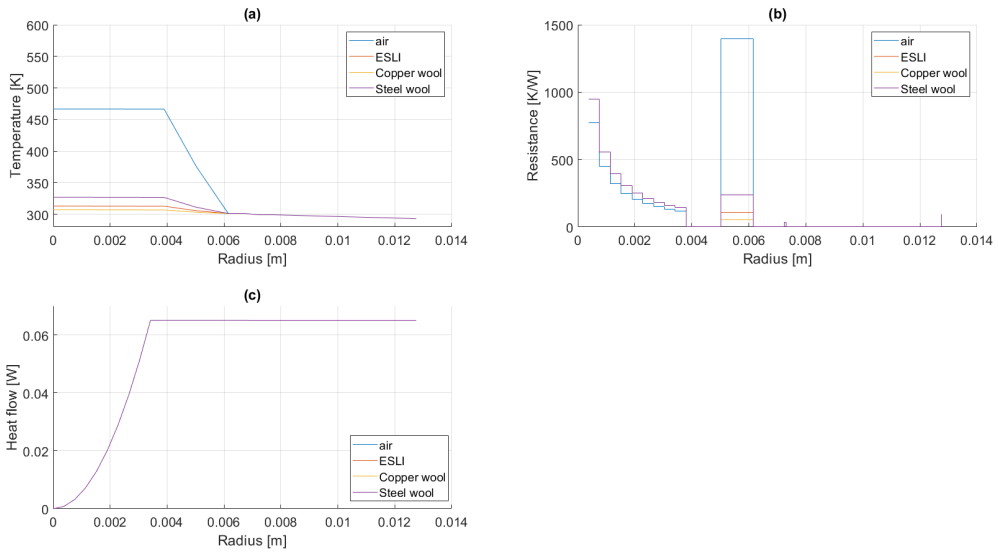

Figure 4.15: Results for different materials in air gap and heat flow of 0.065 W for 8x 1MC06-007

gap are chosen, it can be seen how the total resistance and thus the maximum temperature in the system is decreased (Figure 4.15). The heat input is not enough to raise the temperatures above 325 K for steel wool, so still, all temperature drops at the air gap and no temperature difference across the modules can be generated. When taking air as a medium filling the air gap out of the system, the heat flow can be increased to a value as high as $q_{in} = 0.55W$, leading to maximum temperatures of slightly above 550 K for steel wool as a filling medium (Figure 4.16). The temperature difference across the TE module measures 15 K at this point and can

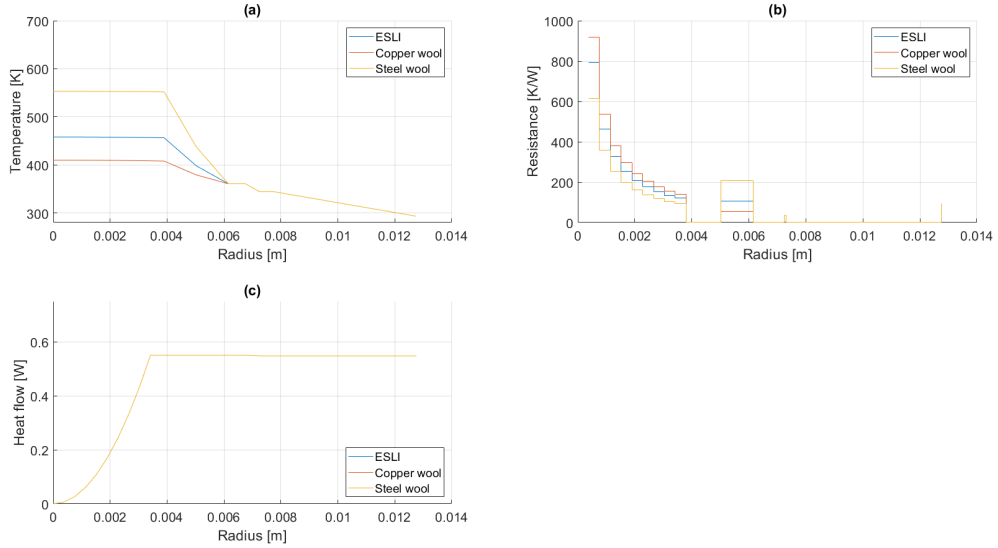

Figure 4.16: Results for different materials in the air gap and heat flow of 0.55 W for 8x 1MC06-007

thus, not be used to generate a notable amount of electrical energy. In 4.3 the assumption was discussed that the exhaust gas does not lose any heat until reaching the EGR because of going immediately from the exhaust opening into the channels. Thus, it seems a reasonable decision to integrate the recirculation after the air gap to increase the temperature before the TE modules. Figure 4.17 shows the results for the same input as in Figure 4.16 but with EGR and that leads to an increase of the temperature drop by about 3 K to 6 K over the TE modules. It turns out, a channel length of 10 mm leads to an exhaust temperature at the channel exit of

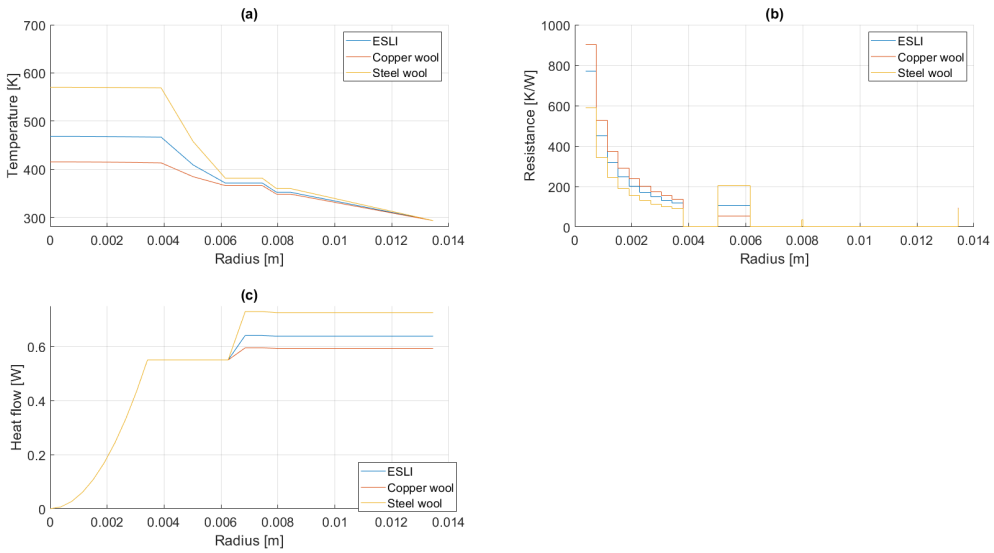

Figure 4.17: Results for different materials in the air gap and heat flow of 0.55 W with EGR for 8x 1MC06-007

well over the required 393 K, so condensation does consequently not take place in that case. Comparing the graphs of the different materials in the previous figures, it shows that thermally copper wool is the best choice because its heat resistance is smaller, so higher heat inputs and higher temperature drops over the modules are possible. With regards to the TE modules the configuration of 8 smaller modules leads to a higher temperature drop than 4 larger modules. The reason for that can be seen in the top right graph of Figure 4.18 where the system is analyzed for copper wool as a filling which enables a heat input of 1.4 W. The 4 modules have a way lower resistance due to their leg geometry and number than the 8 modules. This shows that the smaller modules are more suitable for a system with high overall heat resistance. That is not only because of being able to place 8 of them around the combustor but also because of their design. In a system with small overall heat resistance, the resistance of the modules can be relatively smaller to achieve the same temperature drop. Modules with a high resistance would in such a case very likely lead to a ΔT larger than their optimum which then could be decreased by a larger resistance of the heat sink. Due to unknown reasons the electric-

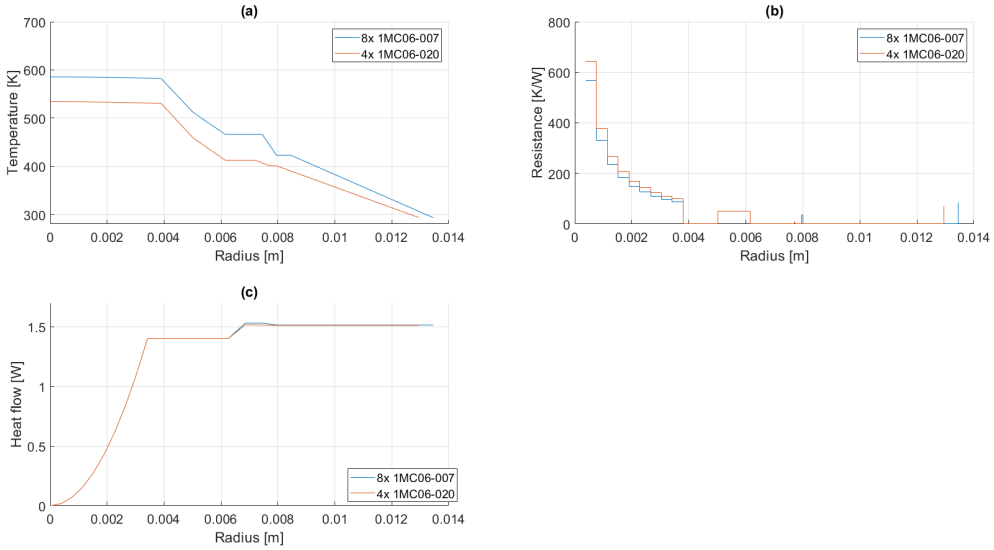

Figure 4.18: Results for copper wool in the air gap and heat flow of 1.4W with EGR (channel length: 10mm) for both TE module configurations

ity generation of the modules does not agree with the data sheet of the manufacturer despite the validation of the equations for the thermoelectric effects with the help of other commercially available modules. It is suspected that the discrepancy originates from material or design changes by the manufacturer that are not accounted for in the used model. That is why it was decided to take the temperature difference across the module as the measurement scale for the performance of the module and aim for the optimum difference given by the data sheets. The optimization of the design with respect to the temperature difference across the TE modules is continued on the basis of copper wool as the filling material for the air gap. In the following, the interdependencies between the variable design parameter and the performance of the TE modules are analyzed. As a first step, it looks at the consequences of changing the design variables of the system which include the number of fins on the heat sink and the channel length of the EGR. The cross-section of the channels is considered to be fixed as cylinders with a variable length. A sweet spot for the channel length exists and is defined by the lower bound being the minimum length necessary to achieve the maximum possible heat transfer into the system. The upper bound is the maximum length possible to not hit the temperature for saturated steam to avoid condensation. In Figure 4.19 the results for different channel lengths are presented.

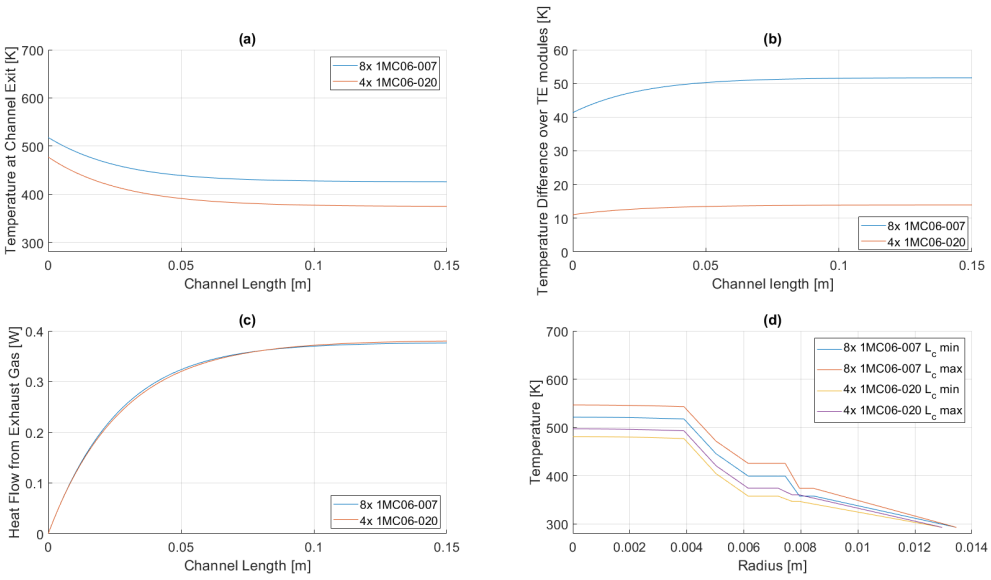

Figure 4.19: Results for copper wool in the air gap and varying the channel length of the EGR

At a heat input of 1.4 W and 20 fins on the heat sink no maximum length for the configuration with 8 modules can be found at which the exhaust temperature at the exit drops below the value of 393 K. For the second configuration that happens at a channel length of 46 mm. The difference in temperature between not using the energy carried by the gas and using the full energy can be seen in Figure 4.19 (d). At the TE modules that increases the temperature by about 10 K and in the chamber that can be even more (up to 25 K) which can improve the catalytic reaction by a lot. Even though the mass flow is assumed to be independent of the heat input from the combustor, the feasible channel length strongly depends on that heat input. That is because it determines the maximum temperature in the system and thus, the entrance temperature of the exhaust gas. As can be seen in Figure 4.20 the more heat input in the combustor the more heat is transferred from the exhaust gas. As long as the entrance temperature of the exhaust gas is the same temperature as that in the combustor, this is valid. However, as soon as the temperature at the entrance is decreased, there will be a heat flow q_{C1} high enough to raise the temperature at the channel above the exhaust gas temperature. That leads to heating the exhaust gas and is to be avoided. Chapter 3.6 mentions another concept for an EGR where the waste heat of the exhaust is used to preheat fuel. An EGR at the TE modules ceases to make sense as soon as q_{ER} drops below the possible heat transfer into the fuel. That needs to be analyzed as soon as a fuel delivery for such a system is developed.

The other design variable, the number of fins on the heat sink, is now analyzed with respect to its effects on the temperature difference over the TE module and the overall temperature distribution. Since the total heat resistance of the system is heavily influenced by the resistance of the heat sink many interactions should be considered. Figure 4.21 depicts the most important ones. Since the overall resistance for a heat sink with

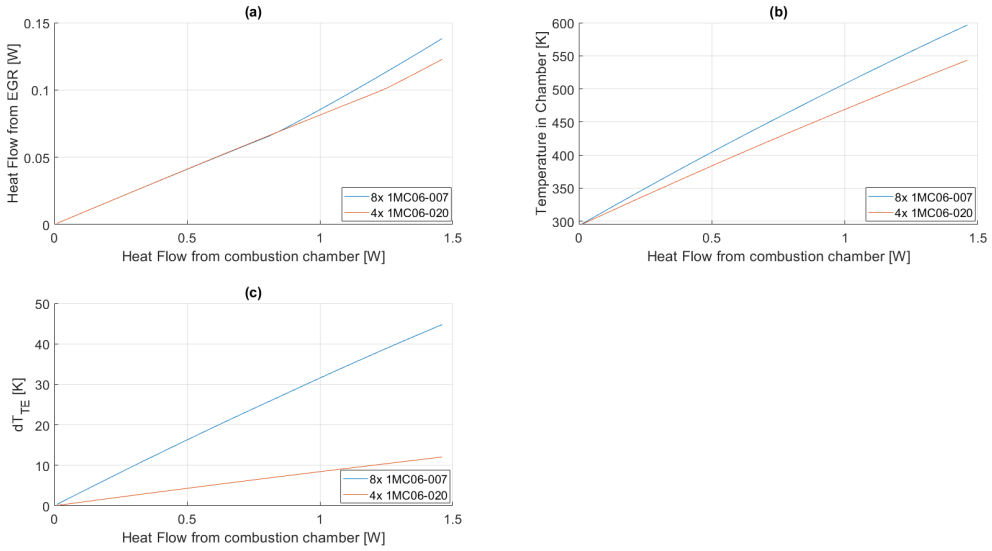

Figure 4.20: Results for copper wool in the air gap and varying heat input q_{C1}

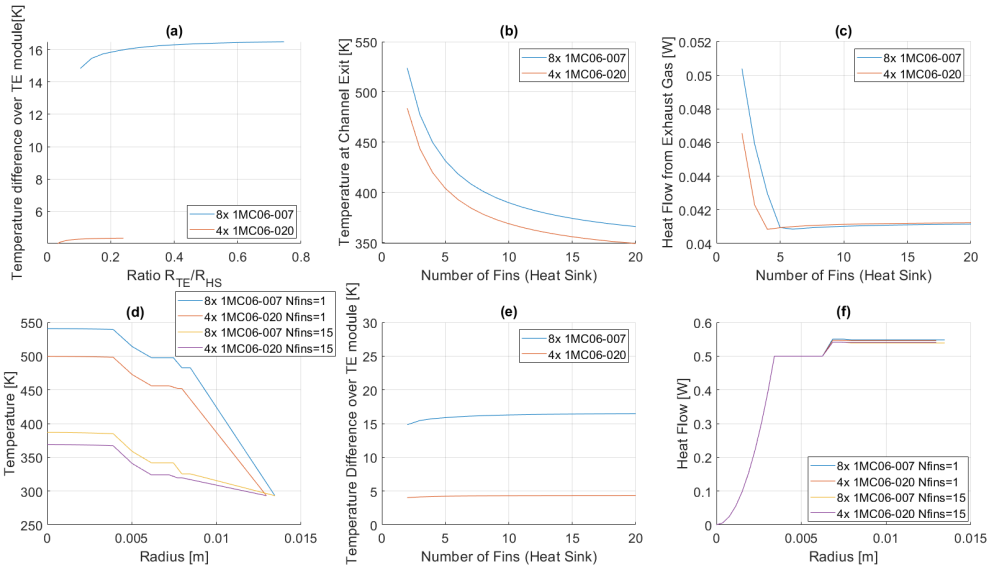

Figure 4.21: Results for varying the number of fins N_f on the heat sink

only 2 fins is higher than for 10 fins which were used to produce all previous results, the heat flow needs to be reduced to 0.5W. It can be seen that the number of fins affects the exit temperature of the EGR channels, so when an optimum for the combination of N_f and L_{ch} is sought, that needs to be taken into account. It turns out that a number of 10 to 15 fins is a good starting point for an optimum design. However, the heat input needs to be increased to bring the temperatures back into the range where condensation is not taking place.

4.7. Sensitivity Analysis

Since the model is solved numerically it makes sense to check for which settings the model converges and if there are limits that need to be taken into account when analyzing the results. The convergence is investigated for the mesh to see whether there is a range of number of elements for which the model becomes unstable. Furthermore, different assumptions have been made that especially refer to some of the coefficients for heat transfer and to make sure these simplifications were permissible the sensitivity of the results to changes in these parameters is analyzed.

Effects of Initial Temperature Guess

To analyze the effects of changing the initial temperature guess the temperature for one component at a time is varied between the lower and upper temperature boundary of 200 and 800 K respectively. For a heat input of 0.25 W, a channel length of $L_{ch} = 10mm$, copper wool as a filling, and 10 fins on the heat sink the algorithm always converges to the same solution after 60 to 80 iterations. It can thus, be said that the convergence of the algorithm is independent of the initial temperature guess.

Sensitivity for Mesh

For the sake of completeness, also the sensitivity of the solution to changes in the mesh shall be investigated. Therefore, the temperature difference over the TE module is analyzed for three different meshes. Only the number of elements for components whose model it allows to change the mesh is varied. For example, for the equations describing the TE module or EGR, a different number of elements is not possible. The results

Component	Mesh 1	Mesh 2	Mesh 3
Combustion chamber	10	50	100
Combustor wall	10	50	100
Air gap	2	2	2
Support structure	10	50	100
Exhaust channel	1	1	1
Exhaust channel wall	10	50	100
Ceramic (TE module)	10	50	100
TE legs	1	1	1
Ceramic (TE module)	10	50	100
Heat Sink	1	1	1
ΔT_{TE} 8x 1MC06-007	32.38275352 K	32.38275376 K	32.38275379 K
ΔT_{TE} 4x 1MC06-020	8.623506395 K	8.623506449 K	8.623506456 K

Table 4.3: Result for ΔT_{TE} for different meshes

for the temperature difference listed in Table 4.3 show that the model is mesh independent.

Sensitivity for Coefficients

Regarding the sensitivity of the solution for coefficients mainly the convective coefficient for air and the heat transfer coefficients for the air gap fillings are important. The convective coefficient for air is not exactly known due to the very unpredictable behaviour of molecules in the air gap and around the heat sink. That is why h_c for air is varied from 2.5 to 17.5 W/m^2K. The results for the temperature difference over the TE module in Figure 4.22 show that for such a wide range the temperature difference only changes by up to 2 K. For the proof-of-concept this is not relevant. With regards to the heat transfer coefficient of the fillings for the air gap, it is also not known how the convection and the geometry of the wool affect the value. Furthermore, the only paper that was found regarding the heat transfer of metallic wools does not in detail describe the model on which the obtained values are based, so instead of reproducing the results the values stated in the

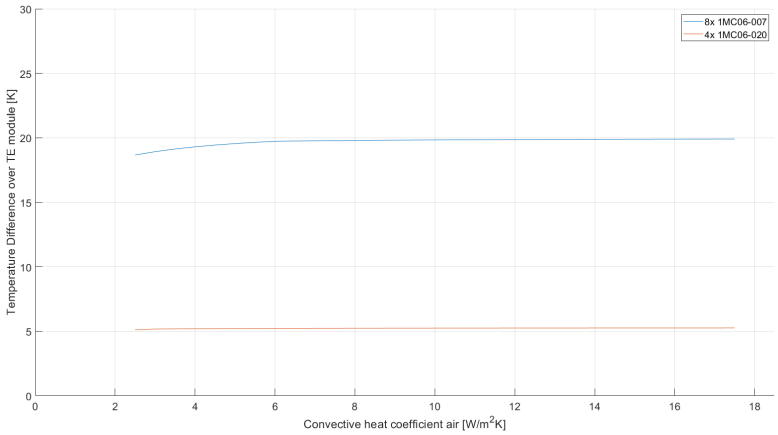

Figure 4.22: Sensitivity of the solution for ΔT_{TE} for changes in h_c

paper have been taken. Therefore, it was decided to take the ESLI fibers as an example and vary their heat transfer coefficient by 20% around the given value. In Figure 4.23 it is shown how the maximum temperature

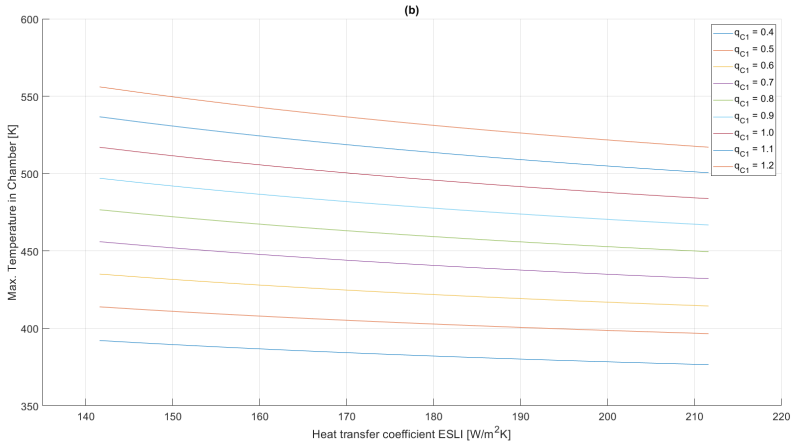

Figure 4.23: Sensitivity of the solution for ΔT_{TE} for changes in the ESLI heat transfer coefficient

in the system depending on the heat input looks like for different values for the coefficient. Especially for high heat inputs the difference can be up to 40 K. It is not expected that the value for the coefficient is so far off the correct value but it is nevertheless, important to be aware of the error that might be introduced by it.

Optimal Design

Now, after investigating the most important interactions between design variables and the heat input at the combustor an optimum design shall be developed with the goal of achieving the maximum temperature difference over the TE modules stated by the manufacturer and if not possible, at least the highest possible temperature difference. Considering the huge difference between a system with 4 or 8 modules, it is obvious that for each configuration its own optimum design needs to be determined. In Figure 4.24 it is shown what the temperature distribution and the heat flows in the two systems look like. The results confirm the expectation that it is despite the optimization not possible to achieve a competitive temperature difference for the 4 modules compared to the 8 modules. The reason is the low heat resistance of the 4 TE modules which could be enhanced by the use of other leg geometries. It can be noted that the smaller the heat resistance of the heat sink the higher ΔT_{TE}. As already proposed by Zhou et al. the heat resistance of the heat sink needs to be minimized until the temperature difference ΔT_{TE} matches the maximum temperature difference for the corresponding module stated by the manufacturer [77]. Since the geometrical parameters of the heat sinks are fixed and it was decided to only manipulate its resistance by changing the number of fins, the resistance is

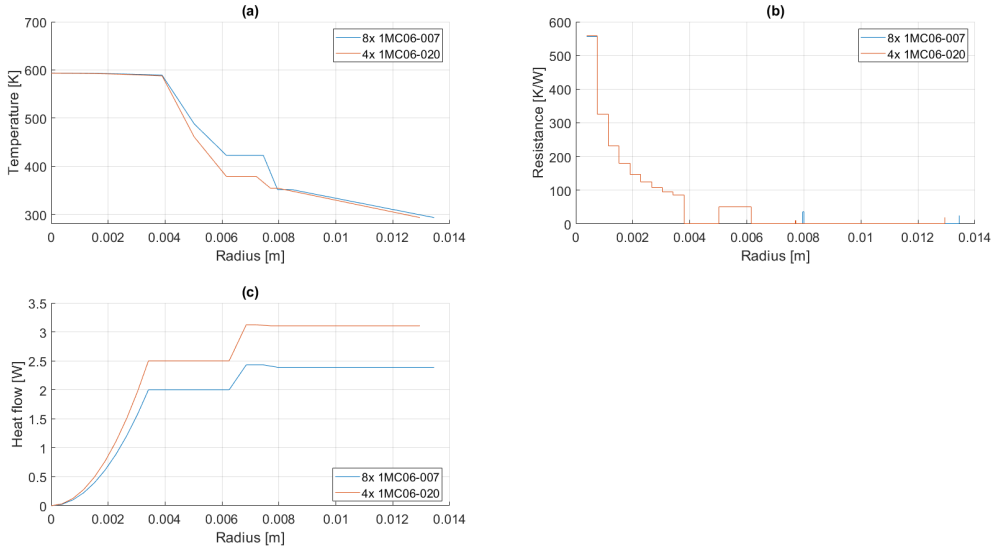

Figure 4.24: Results for the system with optimized parameters

Configuration	8x 1MC06-007 (Configuration 1)	4x 1MC06-020 (Configuration 2)
Goal: ΔT_{TE}	71 K	70 K
Heat loss combustor	2.92 W	2.92 W
Heat input q_{C1}	2 W	2.5 W
Channel length L_{ch}	43 mm	75 mm
Number of fins N_f	39	39
	Results	
ΔT_{TE}	71.2 K	24.4 K
UA product (system)	1.3575e-05 W/K	1.3777e-05 W/K
Required UA product for top & bottom	2.952e-05 W/K	8.1897e-05 W/K
Total UA product	4.3095e-05 W/K	9.5674e-05 W/K
$T_{2_{ex}}$	455 K	393.6 K
R_{TE}	36.2 K/W	9.5 K/W
R_{HS}	24.4 K/W	19.7 K/W
I_{TE}	62.1 mA	56.1 mA
Vn_{TE}	0.66 V	0.32 V
P_{TE}	40.8 mW	18.1 mW
Efficiency (without combustor)	2.04%	0.07%

Table 4.4: Optimum design parameters

limited by how many fins can be placed on the given area. For both cases, this space was exhausted by setting N_f to 39. Regarding the channel length for the EGR, 43 mm was sufficient to achieve the goal of $\Delta T_{TE} = 71K$ over the 8 modules. For the configuration with 4 modules the entire available temperature difference over the channels with a length of 75 mm was not enough to push the temperature difference over 25 K. The calculated total power output summed up over the 8 modules is 40.8 mW. There is not much known about the flight control and the onboard sensors of the FWMAV but to put the power output of the modules into perspective, embedded microcontroller units operate in the range of milliwatts. De Croon states about the DelFly in 2015 that the entire FWMAV requires 3 W to power the motor and electronics where the motor delivers a power of 1.5 W at an efficiency of around 60% [12]. That means the majority (around 2.5 W) of the supplied power is used for the motor and only 500 mW for the electronics. In the case of the chemical actuator, the power for the motor is generated entirely by the chemical reaction and thus, only the electronics need to be powered by an electrical power source. Nevertheless, the TE modules seem to not deliver enough power to go completely without an additional battery. From the available 2.92 W of heat flow through the combustor wall at least the heat input q_{C1} in Table 4.4 must be directed into the system by designing the UA product. That means, for the given actuator the system of TE modules needs to achieve an efficiency of around 17% to deliver the required power of 500 mW.
In Figure 3.15 where the heat flows in the system are depicted it was decided to only look at radial heat flows and neglect the ones leaving the cylindrical structure at the top and bottom. Consequently, the horizontal heat flow can be manipulated by changing the ratio of the heat transfer coefficient in radial and vertical direction. For the here-used heat flows 31.5% of the available heat flow is lost through the top and bottom for configuration 1 and 14.4% for configuration 2. The required UA product for the top and bottom is given and can be achieved by developing suitable insulation. The overall UA product for the entire actuator is then the sum of these two UA products. Guido Mous found out that at least a UA product of 0.1 W/K is required to achieve a flight time of over 10 minutes [27]. That means that the proposed system insulates the actuator well enough to increase the efficiency of the combustion remarkably. It should be noted, however, that the underlying calculations are based on the mass of the combustion chamber only and do not take the increase in mass due to the proposed system into account.

4.8. Discussion

Since the results have already been interpreted and brought into an optimal design, here, the limitations of the model shall be discussed and subsequently, the results summarized in recommendations for the model and the system design. The model is subject to various assumptions and simplifications to be able to apply the described equations and coefficients. Even though the model was able to fulfil its purpose of being proof-of-concept and of giving a basic understanding of design choices for a hybrid system of mechanical and electrical power generation in a micro actuator, it should be further refined and most importantly, experimentally validated. It is not expected that the limitation to 1D changed the results majorly but nevertheless, an extension to at least 2D would be a reasonable step. That would improve especially the prediction of the temperature at the components modelled as a circular arrangement of plane walls. In that way, the influence of the growing gap at the corner of these components on the heat loss could be investigated. The results show that inserts of different porous materials can indeed increase the heat transfer across an air gap but the quality of these results is strongly dependent on how much is known about the air movement and the geometry of the porous media. Further research in that direction should relate the thermal properties to the stiffness properties of the material to analyze its effects on the movement of the actuator. The amount of ongoing research on the design of exhaust channels to use the exhaust's heat energy shows the relevance of that topic. Usually, the EGR is used to preheat fuel but in this project, it was shown that hybrid systems enable using the waste heat to have an additional heat input for the TE modules. It turns out that the channels for the proposed design need to be long compared to the size of the system so that the optimization of the geometry can be further investigated. With regards to the TE modules, it was not possible to relate the output of the ideal model with the data sheets of the modules which is very likely due to many unknown design choices by the manufacturer that influence the electricity generation. That also counts for the equations based on the effective properties presented in 4.3 and a model proposed by Yongija Wu et al. [68] which were tried to be implemented. It should also be noted that the convective coefficient for air at the heat sink can vary a lot when taking into account that the system could be used in devices in motion, like drones. That makes the air stream at the heat sink and thus, its heat transfer dependent on values like the speed and direction of the drone.

Recommendations

From the presented optimum design result different recommendations regarding the design of a hybrid system consisting of a MICE and modules for electricity generation.

1. Increase the relative heat resistance of the TE modules. That can be done in two ways. First, the resistance of all other components should be minimized, for example, by using conductive materials or the proposed fillings to bridge air gaps in the system. Contact resistances should be reduced by using thermal paste or other conduction-enhancing materials. It should be noted that by reducing the overall heat resistance in the described way, the generated temperature drop over the domain decreases for constant heat flow. Secondly, the temperature drop over the modules can be increased by choosing a leg geometry that leads to higher resistance of the TE modules. Also, with regards to real TE modules where the air between the legs transfers heat via convection, insulating materials could be used to fill these gaps and thus, reduce the bypass of heat.

2. Replace the heat sink by cooling the cold side of the TE module with the fuel. In that way, the mass of the system could be reduced by replacing the heat sink with a network of channels for the fuel and at the same time preheating the fuel to increase the catalytic reaction.

3. Optimize the EGR. It was found that the exhaust stream carries a notable amount of energy out of the system which could be used to increase the system's efficiency. Analyzing the optimum design parameters in Table 4.4 with respect to the EGR it can be seen that the channel length L_{ch}, necessary for transferring the heat, tends to be large compared to the length of the actuator with 4.32 mm. Here it makes sense to conduct more research with a focus on the exhaust flow dynamics, perhaps including simple CFD analysis to optimize the channel shape. The shape optimization could either have the goal to reduce the length necessary to transfer the heat or it could aim towards fitting a channel of such a length in the given design space. Furthermore, it turns out that not always the entire energy from the exhaust gas is needed to achieve the wanted temperature difference over the modules. In such a case the rest energy of the gas should be used to preheat the fuel before it enters the combustion chamber. An ideal design could circulate the fuel across the cold side of the TE module as already described and then pass a heat exchanger that uses the remaining energy of the exhaust gas to preheat the fuel even further.

4. Formulate an optimization problem to automate the search for an ideal combination of the design variables. That simplifies finding an optimum and enables the integration of more design variables. Interactions between variables could be visualized in a better way. An important extension of the model would be to introduce a radial and height coordinate to include the heat loss on the top and bottom of the design. It turned out to be an important factor influencing how much heat flows through the attached components and consequently, determines the available temperature difference for the modules.

5. Design an experiment to validate the results of the proposed model and possible extensions. The experiment should especially include measurements regarding the heat transfer of the proposed fillings to get a more precise value for their heat transfer coefficient. The quality of this value would presumably be higher and easier to obtain than developing a model for it since that would have to take a lot of effects into account to be accurate.

4.9. Conclusion

After presenting the results and discussing them by working out recommendations, now the most important points are summarized in an intermediate conclusion. The proposed design for insulating the compliant combustion chamber of a chemical actuator for an FWMAV was simulated in a one-dimensional steady-state heat resistance model and then solved numerically. The model includes a constant heat generation obtained from integrating the time-dependent signal calculated by Guido Mous [27]. The heat transfer coefficients of different porous media inserts to transport this heat with as little resistance as possible towards the TE modules have been implemented. It also solves a system of equations describing the behaviour of the EGR. The model shows that copper wool as the material with the lowest heat resistance enables the highest heat flows. It consequently, reduces the resistance of the air gap so much that the relative resistance of the TE modules is high enough to generate a notable ΔT.The implemented EGR to increase the use of waste heat was, as expected, able to increase the temperature of the system.

5

Transient Heat Resistance-Capacitance Model

During the analysis in steady state, it became clear at some points that looking at the transient behaviour of the system might offer some important insight. One reason to believe that is that the input signal generated by the combustion chamber is time-dependent. It would be interesting to see how the temperature distribution within the system reacts to that and what effects that has on the energy generation by the TE modules. The most important question that shall be answered by adding the time dimension is how long it is going to take the system to heat up to steady state. Especially for the application in FWMAV that is crucial because as opposed to, for example, IoT sensors these drones are often used for short-term operations. That means, the quicker the system heats up and reaches its full potential regarding electrical power generation the better. It was decided to build the transient model based on the resistance-capacitance formulation considering that it was already working with heat resistances for the steady-state model and the calculation is similar. Moreover, it seems to be an often applied method that is easily applicable to a variety of problems [43].

5.1. Equations

Before starting the analysis a method needs to be selected. The problem can either be formulated in an explicit or implicit formulation where the former solves the equation for the next time step based on the solution for the current time step. The latter is working with equations that describe the following steps rather than known values from the steps before. The advantages of using the explicit method are easier mathematical implementation and less required computing power, so it seems to be the better choice for a 1D problem. Being in 1D means again that only variations in radial direction are considered and thus $\Delta\phi = 360° = 6.28$ rad and $\Delta z = L = 4.32$ mm. Every node in the discretization of the domain gets a volume with a thermal capacitance assigned to it. Between the nodes are the resistances, just as already described in steady state (Figure 5.1) [43]. From the energy balance over the node the following equations results

$$T_m^{t+1} = \left(1 - \frac{\Delta t}{C_m} \sum_n \frac{1}{R_{mn}}\right) T_m^t + \left(\dot{Q}_v''' \Delta V_m + \sum_n \frac{T_n^i}{R_{mn}}\right) \frac{\Delta t}{C_m}, \tag{5.1}$$

to determine the node's temperature. From the fact that the first term is not allowed to turn negative, the stability criterion for the time step emerges.

$$\Delta t \leq \left(\frac{C_m}{\sum_n (1/R_{mn}))}\right)_{min}. \tag{5.2}$$

This stability criterion needs to be fulfilled for every node, so the one with the smallest ratio of C_m and the sum of the reciprocals of all resistances determines the time step. The resistances are set up similarly to the steady-state model. For the internal resistances, the underlying equations for the plane wall and for cylindrical coordinates are the following. R_{m+} denotes here the heat resistance in positive radial direction and R_{m-}

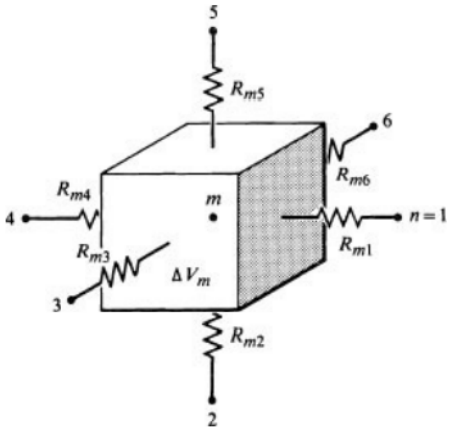

Figure 5.1: Node surrounded by the finite control volume with resistances for the resistance-capacitance formulation [43]

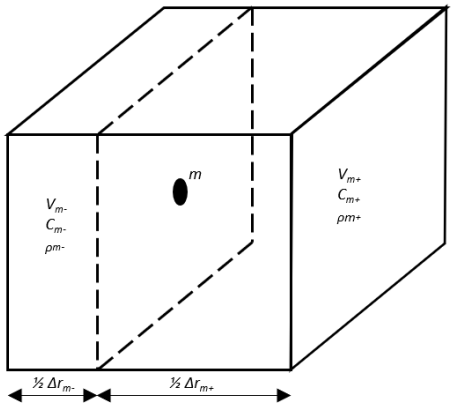

Figure 5.2: Node at an interface surrounded by a finite control volume consisting of half volumes of two adjacent components

	Coordinate System	
	Cartesian	Cylindrical
Coordinates	x, y, z	r, ϕ, z
Indices	m	m
Volume element	$\Delta x, \Delta y, \Delta z$	$r_m, \Delta r, \Delta\phi, \Delta z$
R_{m+}	$\frac{\Delta x}{\Delta y \Delta z k}$	$\frac{\Delta r}{(r_m+\Delta r/2)\Delta\phi\Delta z k}$
R_{m-}	$\frac{\Delta x}{\Delta y \Delta z k}$	$\frac{\Delta r}{(r_m-\Delta r/2)\Delta\phi\Delta z k}$

Table 5.1: Heat resistances for resistance-capacitance formulation [43]

the one in negative radial direction. For convection and radiation the resistances are described as

$$R_c = \frac{1}{h_c \Delta x}, \tag{5.3}$$

$$R_r = \frac{1}{A_n \mathscr{F}_{mn} \sigma \left(T_n^2 + T_m^2\right)(T_n + T_m)} \tag{5.4}$$

where $\mathscr{F}_{mn}$ is the transfer factor which is defined by the geometry and emittances of the surfaces that form the enclosure in which the radiation is to be calculated. Its calculation can be simplified because in the considered case the outer participating surface encloses the inner surface due to the cylindrical shape. For the components where radiation plays a role, especially the air gap, it can be assumed that the outer surface is large compared to the inner surface. That allows setting $\mathscr{F}_{mn} \approx \epsilon_m$. The standard equation for the volume in a cylindrical coordinate system is

$$\Delta V_m = r_m \Delta r \Delta\phi \Delta z. \tag{5.5}$$

But in the considered case components with the shape of a planar wall are arranged in a cylindrical way around the combustor, so their volume element is calculated by

$$\Delta V_m = N \Delta r \Delta z L_{TE} \tag{5.6}$$

where N is the number of modules around the combustor chamber because their surface equals the one of the EGR and heat sink (Figure 4.1) and L_{TE} is the width of the attachments. From that, C_m can be obtained by

$$C_m = \rho c_m \Delta V_m \tag{5.7}$$

with c_m [J/kg K] being the volumetric heat capacity. Since the system consists of multiple components the mentioned equations for the volumes and capacitance can only be applied to the inner nodes of each component. That is because they are based on the assumption that the nodes are of homogeneous material

properties and that all Δr are equal. However, the temperatures at the contact points between different components are particularly interesting, especially with respect to the TE modules where the temperatures at the transition from the ceramics to the legs need to be known. The consequence of placing nodes at these contact points is that one side of the volume is defined by the geometry and material of the component on this side and the volume on the other side by the other component. To cope with this and be able to place nodes at the interfaces, the volumes were set up analogously to the resistances having a finite Volume V_{m+} and thus C_{m+} in positive radial direction and V_{m-} and C_{m-} in negative radial direction for each node. Consequently, each Δr, which is component specific, is divided by two, meaning that each finite volume part is half of the respective component's normal finite volume for inner nodes (Figure 5.2). Nevertheless, for continuity reasons, the volume of the interface nodes needs to be treated as the sum of the two partial volumes. Understanding it as there are two surface nodes at the same position with the boundary condition of having the same temperature and location is, therefore, not enough. The same goes for the capacities which cannot be handled like two separate serial capacities in an electrical circuit but like parallel ones because the result would be two new nodes and a linear temperature distribution within a node is assumed [43].

5.2. Components

In the following, the components that require different or additional equations are explained but generally the principles developed in steady state can also be applied in transient due to the same approach of using resistances.

Combustor & Combustor Wall

The volume of the combustor is calculated with the equation for cylindrical volume elements, assigned with the heat capacity of steam. As an input, the function from Figure 3.13 was taken and discretized for the time steps obtained from the stability criterion and then inserted into equation 5.1. The combustor wall is taken into account as the standard resistance without heat generation under consideration of the special treatment for the interfaces.

Air Gap

Here, radiation is included as a resistance based on equation 5.4 but furthermore, the calculation for the air gap is also solely based on the cylindrical model similar to steady state.

Exhaust Gas Recirculation

The element number for the EGR channel is reduced to 1 so that the inner temperature can be taken to calculate the outer temperature of the channels by equation 5.1 with $\dot{Q}_v''' = \dot{Q}_{ex} = \dot{m} c_p \left(T_{1_{ex}} - T_{2_{ex}}\right)$. $T_{2_{ex}}$ is again obtained with equation 4.35.

TE modules

Gurjinder Singh investigated whether the equations for TE modules derived for steady state are also valid when looking at a transient problem. He found out that the discussed equations can still be used. The electrical response of the modules is so fast compared to the temperature changes that it can be assumed that the temperature difference in one moment of time generates the corresponding electrical energy instantly [29].

Heat Sink

The resistance of the heat sink is calculated as described in 4.3. That means with regards to Figure 5.2 the right side of the node is equal to the volume and thermal capacitance of the entire heat sink while the left side is half of the volume of the ceramic nodes from the TE modules.

5.3. Model Workflow

As opposed to the model for steady state the problem does not have to be solved iteratively because equation 5.1 delivers the solution directly. As can be seen in Figure 5.3 there is only a loop over the time steps. No stability analysis has to be conducted since the problem is inherently stable if the stability criterion is implemented. The working principle of the processes (orange) stays the same, which means the coefficients are still temperature dependent and the only difference with regards to the calculation of the resistances and temperatures is that now the equations for the resistance-capacitance formulation are applied. For the deter-

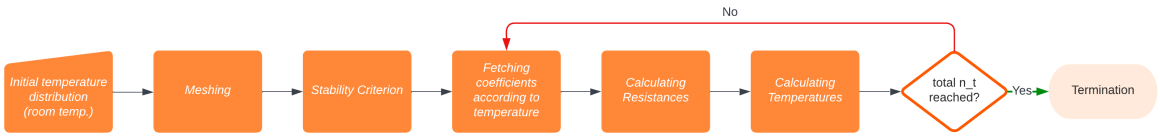

Figure 5.3: Flowchart showing how the temperatures in the system are calculated by the transient model

mination of Δt the stability criterion is evaluated at 5 different temperatures across the possible temperature range and then the minimum is taken.

5.4. Verification

For the verification of the transient model, the same applies as for the steady-state model. It was not experimentally verified. To see whether the algorithm works, a simplified version was implemented and the results were compared to an example in Mills [43, ex. 3.17].

> *"A long, 9 cm-diameter ceramic rod, initially at 20°C, is exposed to a radiation heat flux on one side such that* $q_s = 5000 cos\phi$, $270° < \phi < 90°$, *and is insulated on the other side,* $q_s = 0$, $90° < \phi < 270°$. *Determine the temperature response of the rod. For the ceramic, take* $\rho = 3000 kg/m^3$, $k = 5 W/mK$, *and* $c = 800 J/kgK$."

The results from the nodal temperatures could be reproduced with the implementation of the described algorithm after extending it to 3D. Figure 5.4 visualizes the problem and defines the distribution of nodes across

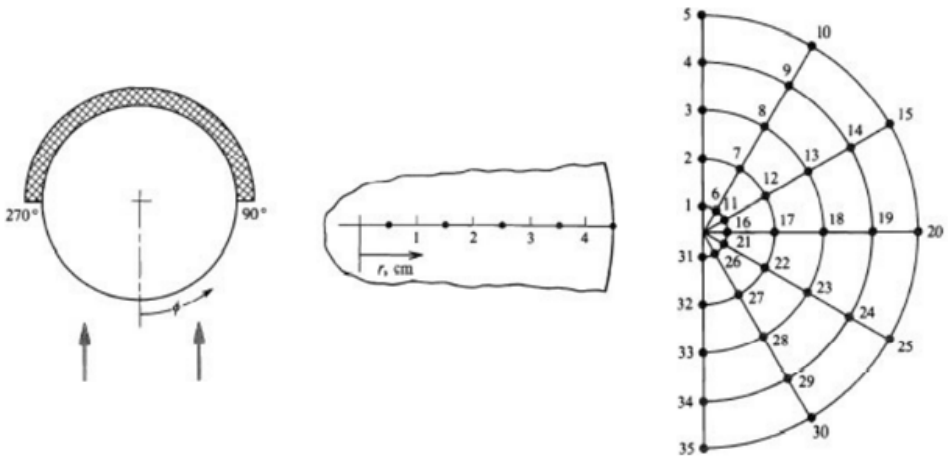

Figure 5.4: Depiction of the example used to verify the algorithm for the resistance-capacitance formulation

the domain. The solution was plotted in a graph and the points of the solution given in Mills were marked in Figure 5.5.

5.5. Results

When the resistances were implemented the stability criterion was evaluated for the described configuration and a time step of about 1e-5 s was obtained. Even using the more efficient linear interpolation tool by Jan Simon and vectorizing the problem did not make the algorithm fast enough to run in reasonable computation time. Unfortunately, the use of parallel programming is not possible since each iteration of the time loop depends on the previous iteration. Even with the cluster Delft Blue, it was only possible to solve the problem for a period of 50 s in a computation time of 120h with an allocated memory of 40 Gb. In Figure 5.6 the graph plotting the results of this calculation can be seen. It should be noted that it is not possible to draw any conclusions about the thermal behaviour from the graph. In Figure 5.7 the final temperature distribution after

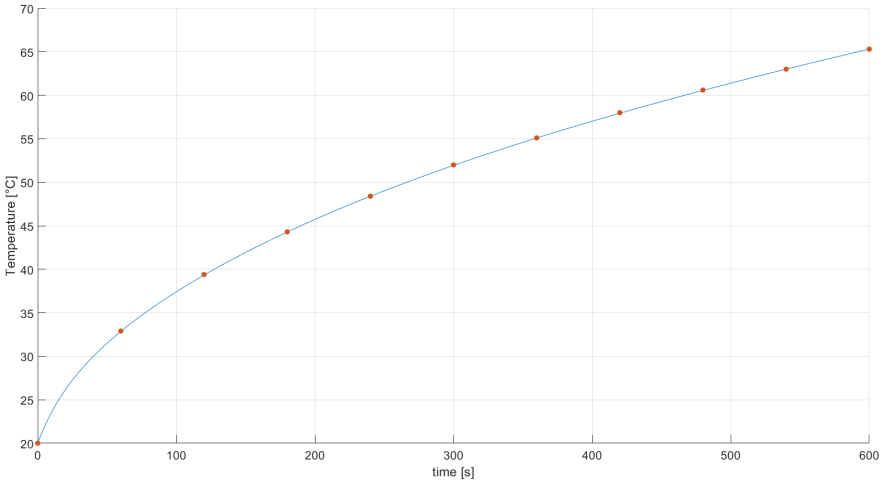

Figure 5.5: Graph of the calculated solution with markers at the solution from Mills [43]

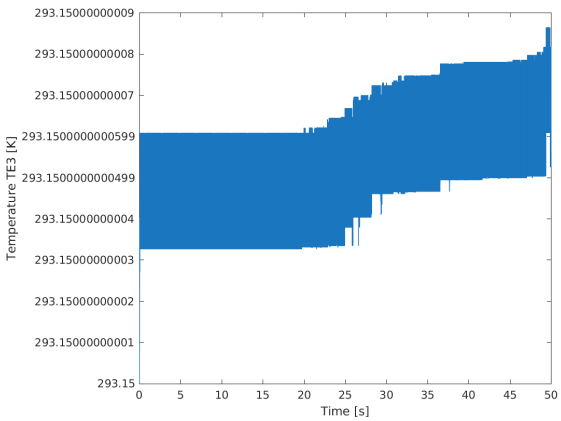

Figure 5.6: Transient response of the temperature after the TE modules for a period of 50 s

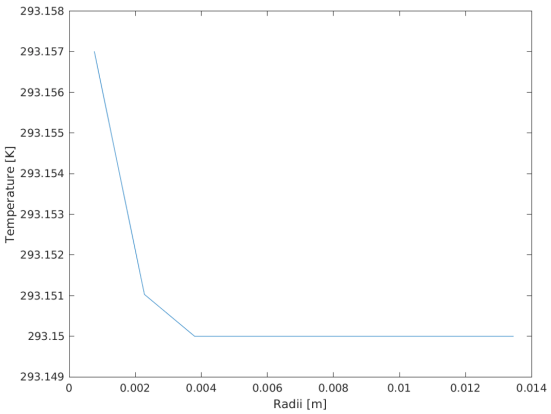

Figure 5.7: Temperature distribution across the domain after 50 s

50 s over r_m is depicted. It can be seen that the temperature drop is mainly over the inside of the combustion chamber because the model does not take into account how the steam is generated. The temperature in the combustion chamber has already very high temperature at the start due to the catalytic reaction. Consequently, it makes sense to either set the inner temperature equal to the temperature function of the chemical reaction or to assign a starting temperature. Nevertheless, the computation time of the model is too long to be practically used. It turns out that using the implicit formulation of the problem would have been the better choice due to being inherently stable. As a consequence, the time step could have been larger, thus, reducing the number of calculations and the computation time dramatically. The most important answer to get out of the model would have been to tell when steady state is reached and a reasonable amount of electrical energy is being generated. Since most of the questions regarding an optimal design can be answered with sufficient quality by using the steady-state model and the limited time for the project, it was decided to not pursue solving the transient problem any further. Instead, the code for the simplified example, described in 5.4 was used and average values for resistances, capacitance and attached coefficients were taken to get an idea of how long it takes to heat up the system to steady state. It should be noted that this result should be treated carefully because due to the average values there is no precise temperature distribution and steady-state temperature to be expected. Figure 5.8 shows the response for the simplified problem where only the

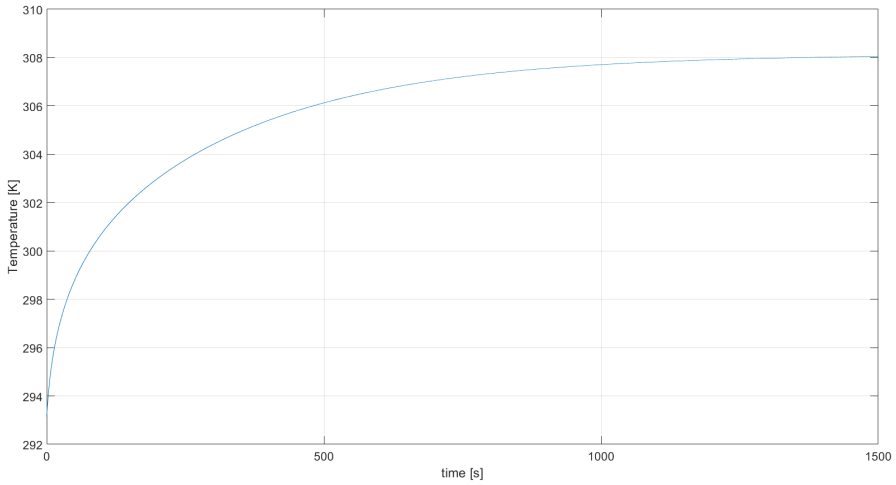

Figure 5.8: Simplified transient response with average values for a heat input of the positive values of $q_{C1} = 2sin(2\pi 30 m\Delta t)W$

positive values of a simple sine with a frequency of 30 Hz and an amplitude of 2 W serve as an input function. For the calculation of the average values, the combustion chamber was not included to take into account that its temperature values increase instantly due to the reaction. The steady-state temperature calculated for the average values is not equal to the temperature calculated in the steady-state model, so an exact prediction of the time the system needs to reach steady state is not possible. It is possible though, to see that even for such a small temperature a cylinder with comparable size and material properties takes up to around 1000 s to reach steady state. Variations in the derived average values do not lead to changes in the graph worth mentioning.

5.6. Discussion

The knowledge about the modelling of each component obtained in the steady-state model was used to implement a transient model based on the explicit method for the resistance-capacitance formulation. It was not possible to optimize the model regarding its computation time within the explicit formulation. That is because the finite volumes of the nodes are so small that in the stability criterion the thermal capacity becomes small relative to the sum of the reciprocals of the resistances. Consequently, the time step becomes so small that many iterations are needed to calculate the temperatures for a certain period of time. That makes the code so inefficient that the analysis of different configurations is impractical. The results from a very simplified version indicate that a comparable system takes around 1000 seconds or 17 minutes to reach its steady state after heating up from ambient temperature. That has consequences for its usability, considering

that, for example, FWMAV have a flight time of only about 10 minutes. First of all, as long as the system is not heated up to its steady state the electrical output or the increase in insulation is not outweighing the increased mass of the system. On top of that, even if at steady state no condensation takes place, that can still be the case in the starting phase of the actuator when the temperature did not reach its steady state yet. That means, because the length of the exhaust channels is adapted to the temperature distribution in steady state, it is very likely that the water carried by the gases condensates and clogs the pipes. Some mitigation for the use in FWMAV could be achieved by preheating the system on the ground with either burning fuel or using heat blankets. However, that is not a practical solution and only makes sense for drones in operations of long duration like in greenhouses where the drones could stop for a refill and then start flying again. The overall efficiency would be decreased when taking into account the energy for preheating, even though the efficiency during one flight would be slightly increased by the insulation and generation of electrical energy. The presented results show that it is necessary to develop a functional and efficient transient model of the system to analyze the temperature distribution after certain periods of time and integrate that into the optimization of the system. In that way, it could be investigated what effects different parameter changes have, also on the time response, because as it shows now, that has a deciding influence on the system design. Remote sensors like the ones for IoT applications are not as affected because the time the system needs to reach steady state is short compared to the operational time of the sensor. Most of the time, there are also not as many restrictions regarding the weight and size of the system, so a larger tank for the fuel could be used to keep the actuator idle when not as much power is needed.

5.7. Conclusion

It was decided to test the thermal response of the system in a transient model to find out from which point in time the optimum output calculated in chapter 4 is reached. After finding out that the explicit formulation of the problem is not suitable due to the high computation time caused by small time steps to keep the model stable, it was not pursued any further. Instead, a simplified model was used to obtain an estimate of the duration and it turned out that it takes around 15 to 20 minutes.

6

Discussion

After interpreting model-specific results in the chapters above, now a general discussion of the project's relevance follows. With the help of a steady-state model (Chapter 4), it was shown that the waste heat of a MICE can, despite a complicated wall geometry of the combustion chamber, be used to create a sufficient temperature difference over TE modules. After optimizing the design in steady state by trying different configurations for the EGR, modules, and heat sink the transient response of the proposed system was analyzed where it turned out that it takes around 15 to 20 minutes to reach steady state.
The models are set up in a way that various components of different geometries can be approximated with fairly simple resistances to give a first approximation of the temperature distribution. That enables easy analysis of the effects of certain parameter changes and consequently gives information about how the system needs to be set up for further proceeding. Especially with the steady-state model, it was possible to answer the research question of whether a hybrid system of a MICE and MTEG can generate a notable amount of electrical energy. Being able to generate the TE module's maximum temperature difference shows that the system is able to use the full potential of the modules. That results in an amount of electrical power that lies in the range of small microcontrollers. Consequently, the model and the concept are valuable results because both are applicable in a wide range of applications.
While FWMAV served as a use case and its applications have already been discussed to a great extent, the potential of the design is certainly not restricted to it. Other kinds of unmanned vehicles and drones could profit as well. Mechanical energy for propellers of small watercraft or robots could be provided and make these machines able to operate for a longer time due to the higher energy density. The size of the actuator system could for example be increased to serve as a power supply for power tools where at the moment lithium batteries or normal combustion engines are most widespread. That includes mowing machines, different kinds of saws or even indoor vacuum cleaners since there are no toxic exhaust gases. As already mentioned, different kinds of IoT sensors could be powered by micro combustion to make them more independent and mobile. The same goes for actuators like pumps. As long as heat input from a given combustor is known, the level of insulation by different wall configurations can be examined and if feasible, the temperature difference over TE modules can be predicted.

7

Conclusion

In the conducted study a concept for a hybrid chemical actuator was proposed to increase the efficiency of chemical microactuators and a model was developed to optimize electricity generation from its waste heat with the help of TE modules.
The actuator, delivering the mechanical energy to power an FWMAV, is based on a compliant combustion chamber and thus, minimizes leakage and friction, two important problems in micro combustion. The energy of hydrogen peroxide as a fuel is released by a catalytic reaction without toxic exhausts to be a sustainable alternative to lithium batteries and to enable indoor usage.
One difficulty regarding the design was to thermally connect the bellow structure of the combustion chamber to the TE modules. That was achieved by conduction enhancement through porous media in the air gap. An advantage of the design concept is that this interface between the combustion chamber and the system is not only restricted to bellow walls but enables the connection to various wall geometries. That, in combination with an EGR to use even more energy from the waste heat, makes the concept feasible to attach TE modules. The generated electrical energy can then be used to power control circuits or increase the life of an onboard battery.

This chapter is used to summarize all findings during the study.

- A one-dimensional steady-state heat resistance model was developed in chapter 4 which serves to calculate the temperature distribution across the domain for different configurations.
- Results were compared using four and eight TE modules of two different sizes.
- For the air gap, the effects of copper wool, steel wool, and ESLI carbon velvets as porous media inserts at the interface between the combustor, compared to air, were analyzed. It was shown that, due to enhanced conduction with those inserts, more waste heat can be used for electricity generation while staying within the material's temperature limits. Furthermore, in that way, the relative resistance of the TE modules is increased so that a higher temperature gradient over the module can be created.
- A simple EGR was implemented and it was shown under which circumstances it makes sense to use it to heat the TE modules or to preheat the fuel. In general, the model indicates that using EGR at the modules can often be necessary to achieve their maximum temperature difference.
- Based on the results for interdependencies between the chosen design values, an optimum design was developed. 2 W of heat input could be turned into a temperature difference of 71 K over the modules which is equal to the maximum ΔT given for that specific module. The ideal equations for thermoelectric phenomena predict a power output of around 41 mW which is in the range of power consumption of microcontroller units.
- Subsequently, a transient model of the system based on the explicit method for a resistance-capacitance formulation was built to determine the time it takes the system to reach steady state and thus, generate the power predicted by the previously described steady-state model. Although a useful model as detailed as the steady-state model could not be created due to its long computation time caused by the stability criterion, a simplified version could provide an answer in a reasonable time.

- It turned out that with needing 15 to 20 minutes to reach steady state the proposed system is only under conditions advantageous for the use in FWMAV because its feasibility increases with the time of its continuous use. It is therewith, suitable for many other applications where continuous use is more widespread, like in remote sensors for example.

Only parts of the model were verified, so another study needs to be conducted to experimentally validate the results. That makes sense to further refine the model. Nevertheless, based on reasoning and by thoroughly keeping track of the simplifications the results were found to be sufficient for an initial proof-of-concept.

7.1. Recommendations

Further research regarding the topic of this study should investigate the use of porous media inserts in more detail because that copper wool is the best choice was only shown for heat flow and temperature drop over the modules. A stiffness analysis of such material in combination with the oscillation of the actuator could reveal that the movement is too impaired. An in-depth analysis could then suggest that another fiber geometry for the copper wool or another material like ESLI carbon velvet is more appropriate. It also seems reasonable to aim for system integration. There are still many unanswered questions about fuel storage and fuel delivery. However, there are some promising solutions proposed in previous work [27][57][30][3] and this project so that a detailed design could be generated which possibly ends up in a first prototype.
To summarize, it can be said that the design concept of a hybrid chemical actuator with TE modules and EGR is a great solution to increase the efficiency of a MICE by both insulating the combustor and using the waste heat to generate electricity. The developed model turns out to be a valuable tool to thermally optimize comparable systems and provides an interesting starting point for further design refinement.

A

Appendix

A.1. Material Coefficients

Material	Conductivity $[W/mK]$ for different temperatures							Reference
	200 K	300 K	400 K	500 K	600 K	700 K	800 K	
Stainless Steel	13	15	17	18	20	21.5	23	[43]
Aluminium	237	237	240	236	231	224.5	218	[43]
NBeTe	1.37	1.37	1.37	1.37	1.37	1.37	1.37	[32]
PBeTe	1.37	1.37	1.37	1.37	1.37	1.37	1.37	[32]
Steam	N.A.	N.A.	0.0269	0.0361	0.0465	0.0578	0.0699	[70]
Copper	413	401	393	386	379	372.5	366	[43]
Aluminium Nitride	650	285	180	138	96	80	75	[51]

Material	Convective coefficients $[W/m^2K]$ for different temperatures							Reference
	200 K	300 K	400 K	500 K	600 K	700 K	800 K	
Air	2.5	2.5	2.5	2.5	2.5	2.5	2.5	[43]
ESLI	85	85	85	85	85	85	85	[49]
Copper wool	177	177	177	177	177	177	177	[56]
Steel wool	38	38	38	38	38	38	38	[56]

Material	Emissivities for different temperatures							Reference
	200 K	300 K	400 K	500 K	600 K	700 K	800 K	
Stainless Steel	0.0707	0.0944	0.1175	0.1308	0.1432	0151	0.1681	[48][67]
Aluminium Nitride	0.85	0.8434	0.89	0.92	0.94	0.95	0.96	[47]

Material	Thermal capacities $[J/kgK]$ for different temperatures							Reference
	200 K	300 K	400 K	500 K	600 K	700 K	800 K	
Stainless Steel	402	477	515	539	557	569.5	582	[43]
Aluminium	798	903	949	996	1033	1089.5	1146	[43]
Copper	356	385	397	412	417	425	433	[43]
Aluminium Nitride	800	910	960	1020	1035	1045	1050	[33]
Steam	1850	1864	1901	1954	2015	2080	2147	[16]

Material	kinematic viscosity $[10^{-6}m^2/s]$ for different temperatures							Reference
	200 K	300 K	400 K	500 K	600 K	700 K	800 K	
Air	7.53	15.69	25.89	37.83	51.29	66.45	82.64	[58]

A.2. Concept Evaluation Table

Concept description	Efficiency Electricity Generation	Efficiency Combustor	Mass/Size	Suitable for Power input	Manufacturability	Reliability	Complexity	Academic Relevance
AIR GAP WITH FILLING								
Metallic wool insert • 95% porosity • 98% porosity	**TE & TPV:** Heat transfer coefficient towards modules is increased (higher temperature at modules) (+) **Piezo:** Does not increase power output of motion (o)	Adding layers to combustor wall insulates combustor. However, wool adds resistance to motion (o)	Adding metallic wool increases mass but increase is negligible (o)	N.A.	Cheap manufacturing from metallic fibers (++)	passive component that would not fail even after many load cycles (++)	Pure metallic wool adds no complexity and requires no special mounting methods (++)	Used in different applications but novel to MICE (+)
ESLI Vel-Therm Gasket	**TE & TPV:** Heat transfer coefficient towards modules is increased (higher temperature at modules) (++) **Piezo:** Does not increase power output of motion (o)	Adding layers to combustor wall insulates combustor. However, fibers adds little resistance to motion (+)	Adding fibers increases mass but increase is negligible (o)	N.A.	complicated manufacturing with precision cutting and anchoring in adhesive (-)	passive component that would not fail even after many load cycles (++)	No special mounting methods but more sensitive in handling (+)	High-tech product and novel to MICE (++)
No insert	**TE & TPV:** High heat transfer coefficient of air gap leads to high temperature drop and low temperature at modules (-) **Piezo:** Better insulation of combustor could lead to higher temperatures and thus, more power output at piezo (+)	An insulation layer of air with a very low transfer coefficient (++)	No mass change (o)	N.A.	N.A.	No additional components (++)	No additional components (++)	N.A.

Table A.1: Explanation 1 for concept evaluation with identified characteristics. Scores: excellent (++), good(+), average (o), poor(-), very poor(–), based on [27]

Concept description	Efficiency Electricity Generation	Efficiency Combustor	Mass/Size	Suitable for Power input	Manufacturability	Reliability	Complexity	Academic Relevance
			Exhaust Gas Recirculation					
Preheating fuel	**TE & TPV:** Temperature in chamber increases and leads to higher efficiency (slightly higher temperature at modules) (+) **Piezo:** Temperature in chamber increases and leads to higher output power from combustor (++)	Temperature inside of the combustor is increased and thus, catalytic reaction accelerated (++)	Necessary components made of heavy materials (-)	N.A.	Small parallel channels in copper plate fairly easy to manufacture (etching) (+)	passive component that would not fail even after many load cycles (++)	requires additional components and optimization of channels (-)	Not new to MICE but optimization is still part of ongoing research (+)
Circulation in support structure	**TE & TPV:** additional heat input at modules increases their hot side temperature (++) **Piezo:** Temperature in chamber increases slightly and leads to higher output power from combustor (+)	additional heat input in wall increases combustor temperature slightly for better catalytic reaction (+)	Necessary components made of heavy materials (-)	N.A.	Small channels in copper plate fairly easy to manufacture (etching) (+)	passive component that would not fail even after many load cycles (++)	requires additional components and optimization of channels (-)	Not new to MICE but optimization is still part of ongoing research (+)
No exhaust gas recirculation	**TE & TPV & Piezo:** High heat losses due to high temperature of exhaust when it leaves the system but lower system weight (-)	low efficiency due to high heat losses in exhaust (-)	No mass increase (o)	N.A.	N.A.	No additional components (++)	No additional components (++)	N.A.

Table A.2: Explanation 2 for concept evaluation with identified characteristics. Scores: excellent (++), good(+), average (o), poor(-), very poor(–), based on [27]

Concept description	Efficiency Electricity Generation	Efficiency Combustor	Mass/Size	Suitable for Power input	Manufacturability	Reliability	Complexity	Academic Relevance
ELECTRICAL POWER GENERATION								
TE module	low electrical conversion efficiencies of around 4% (-)	additional wall that increases overall heat transfer coefficient to surroundings (+)	heavy components and additional system changes necessary (wiring, mounting etc.) (–)	Low temperature of catalytic reaction is perfect because it is in operating temperature of TE modules (++)	Cheap off-the-shelf modules available (++)	passive component that would not fail even after many load cycles, also no moving parts (++)	requires additional components but the module itself is simple (+)	Not new to micro generators but use for MICE is novel (+)
TPV module	low electrical conversion efficiencies of around 6% (-)	additional wall that increases overall heat transfer coefficient to surroundings (+)	heavy components and additional system changes necessary (wiring, mounting etc.) (–)	Wavelengths of thermal radiation at low temperatures too low for modules, so it only heats them up (–)	Modules are fairly expensive and consists of different components (filter, cells etc) (o)	passive component that would not fail even after many load cycles, also no moving parts but too much heat due to low wavelengths (+)	requires additional components and module itself is rather complex (o)	Not new to micro generators but use for MICE is novel (+)
Piezoelectric mechanism	Comparably high conversion efficiencies of around 37% (+)	Does not directly decrease combustion efficiency but adds resistance to motion (o)	heavy components and additional system changes necessary (wiring, mounting etc.) (–)	Implementation would be possible making use of oscillations from chamber but heat loss would not be decreased (-)	Components fairly cheap commercially available (+)	component that would not fail even after many load cycles (+)	requires additional components and connection to oscillation of chamber rather difficult (-)	Not new to micro generators but use for MICE is novel (+)

Table A.3: Explanation 3 for concept evaluation with identified characteristics. Scores: excellent (++), good(+), average (o), poor(-), very poor(–), based on [27]

Bibliography

[1] Jeongmin Ahn, Craig Eastwood, Lars Sitzki, and Paul D. Ronney. Gas-phase and catalytic combustion in heat-recirculating burners. *Proceedings of the Combustion Institute*, 30(2):2463–2472, 1 2005. ISSN 1540-7489. doi: 10.1016/J.PROCI.2004.08.265.

[2] H. T. Aichlmayr, D. B. Kittelson, and M. R. Zachariah. Miniature free-piston homogeneous charge compression ignition engine-compressor concept—Part I: performance estimation and design considerations unique to small dimensions. *Chemical Engineering Science*, 57(19):4161–4171, 10 2002. ISSN 0009-2509. doi: 10.1016/S0009-2509(02)00256-7.

[3] A.J.H. Meskers. *High energy density micro-actuation based on gas generation by means of catalysis of liquid chemical energy*. PhD thesis, Delft University of Technology, Delft, 10 2010.

[4] B. Aravind, Karan Hiranandani, and Sudarshan Kumar. Development of an ultra-high capacity hydrocarbon fuel based micro thermoelectric power generator. *Energy*, 206:118099, 9 2020. ISSN 0360-5442. doi: 10.1016/J.ENERGY.2020.118099.

[5] Bahamin Bazooyar and Hamidreza Gohari Darabkhani. Analysis of flame stabilization to a thermophotovoltaic micro-combustor step in turbulent premixed hydrogen flame. *Fuel*, 257:115989, 12 2019. ISSN 0016-2361. doi: 10.1016/J.FUEL.2019.115989.

[6] Caspar Titus Bolsman. *Flapping wing actuation using resonant compliant mechanisms*. PhD thesis, Technische Universiteit Delft, 2010.

[7] Rei Yu Chein, Yen Cho Chen, Che Ming Chang, and J. N. Chung. Experimental study on the performance of hydrogen production from miniature methanol–steam reformer integrated with Swiss-roll type combustor for PEMFC. *Applied Energy*, 105:86–98, 5 2013. ISSN 0306-2619. doi: 10.1016/J.APENERGY.2012.12.040.

[8] Loy Chuan Chia and Bo Feng. The development of a micropower (micro-thermophotovoltaic) device. *Journal of Power Sources*, 165(1):455–480, 2 2007. ISSN 0378-7753. doi: 10.1016/J.JPOWSOUR.2006.12.006.

[9] Zhang Chunbo and Khaliland Bernal Luis P.and Washabaugh Peter D Najafi. An Integrated Combustor-Thermoelectric Micro Power Generator. In Ernst Obermeier, editor, *Transducers '01 Eurosensors XV*, pages 34–37, Berlin, Heidelberg, 2001. Springer Berlin Heidelberg. ISBN 978-3-642-59497-7.

[10] Werner J.A. Dahm, Jun Ni, Kevin Mijit, Rhett Mayor, George Qiao, Anish Benjamin, Yongxian Gu, Yong Lei, and Melody Papke. Micro internal combustion swing engine (MICSE) for portable power generation systems. In *40th AIAA Aerospace Sciences Meeting and Exhibit*, 2002. doi: 10.2514/6.2002-722.

[11] G.C.H.E. de Croon, K.M.E. de Clercq, R. Ruijsink, B. Remes, and C. de Wagter. Design, Aerodynamics, and Vision-Based Control of the DelFly. *International Journal of Micro Air Vehicles*, 1(2), 2009. ISSN 1756-8293. doi: 10.1260/175682909789498288.

[12] G.C.H.E. de Croon, M. Perçin, B.D.W. Remes, R. Ruijsink, and C. De Wagter. *The DelFly*. 2016. doi: 10.1007/978-94-017-9208-0.

[13] Sagar B Mane Deshmukh, A Krishnamoorthy, and Virendra K Bhojwani. Experimental investigations of effect of depth of Swiss roll combustor on its thermal performance as a heat generator. *International Journal of Ambient Energy*, 40(7):704–715, 2019. doi: 10.1080/01430750.2017.1423377. URL https://doi.org/10.1080/01430750.2017.1423377.

[14] Jiaqiang E, Jiangjun Ding, Jingwei Chen, Gaoliang Liao, Feng Zhang, and Bo Luo. Process in micro-combustion and energy conversion of micro power system: A review. *Energy Conversion and Management*, 246:114664, 10 2021. ISSN 0196-8904. doi: 10.1016/J.ENCONMAN.2021.114664.

[15] Diana Enescu. Thermoelectric Energy Harvesting: Basic Principles and Applications. In Diana Enescu, editor, *Green Energy Advances*, chapter 1. IntechOpen, Rijeka, 2019. doi: 10.5772/intechopen.83495. URL https://doi.org/10.5772/intechopen.83495.

[16] Engineering ToolBox. Water Vapor - Specific Heat vs. Temperature, 2005. URL https://www.engineeringtoolbox.com/water-vapor-d_979.html.

[17] A. H. Epstein and S. D. Senturia. Macro power from micro machinery, 1997. ISSN 00368075.

[18] A. H. Epstein, S. D. Senturia, O. Al-Midani, G. Anathasuresh, A. Ayon, K. Breuer, K. S. Chen, F. F. Ehrich, E. Esteve, L. Frechette, G. Gauba, R. Ghodssi, C. Groshenry, S. A. Jacobson, J. L. Kerrebrock, J. H. Lang, C. C. Lin, A. London, J. Lopata, A. Mehra, J. O.Mur Miranda, S. Nagle, D. J. Orr, E. Piekos, M. A. Schmidt, G. Shirley, S. M. Spearing, C. S. Tan, Y. S. Tzeng, and L. A. Waitz. Micro-heat engines, gas turbines, and rocket engines the mit microengine project. In *28th Fluid Dynamics Conference*, 1997. doi: 10.2514/6.1997-1773.

[19] Alan H. Epstein. Millimeter-scale, MEMS gas turbine engines. In *American Society of Mechanical Engineers, International Gas Turbine Institute, Turbo Expo (Publication) IGTI*, volume 4, 2003. doi: 10.1115/GT2003-38866.

[20] European Commission. Study on the EU's list of Critical Raw Materials - Final Report. Technical report, 2020.

[21] L. G. Ferguson and L. M. Fraas. Theoretical study of GaSb PV cells efficiency as a function of temperature. *Solar Energy Materials and Solar Cells*, 39(1):11–18, 11 1995. ISSN 0927-0248. doi: 10.1016/0927-0248(95)00030-5.

[22] A. Carlos Fernandez-Pello. Micropower generation using combustion: Issues and approaches. *Proceedings of the Combustion Institute*, 29(1):883–899, 1 2002. ISSN 1540-7489. doi: 10.1016/S1540-7489(02)80113-4.

[23] Claudio Ferrari, Francesco Melino, Michele Pinelli, and Pier Ruggero Spina. Thermophotovoltaic energy conversion: Analytical aspects, prototypes and experiences. *Applied Energy*, 113:1717–1730, 1 2014. ISSN 0306-2619. doi: 10.1016/J.APENERGY.2013.08.064.

[24] Kelvin Fu, Aaron J. Knobloch, Fabian C. Martinez, David C. Walther, Carlos Fernandez-Pello, Al P. Pisano, Dorian Liepmann, Kenji Miyaska, and Kaoru Maruta. Design and Experimental Results of Small-Scale Rotary Engines. In *Micro-Electro-Mechanical Systems (MEMS)*, pages 867–873. American Society of Mechanical Engineers, 11 2001. ISBN 978-0-7918-3555-5. doi: 10.1115/IMECE2001/MEMS-23924.

[25] Gustaaf Goor. Hydrogen Peroxide: Manufacture and Industrial Use for Production of Organic Chemicals. 1992. doi: 10.1007/978-94-017-0984-2{_}2.

[26] Darren Vincent Green. *Development of a Piezoelectric Micro Engine Using Pulsed Catalytic Combustion*. PhD thesis, The Pennsylvania State University, 12 2008. URL https://etda.libraries.psu.edu/catalog/9282.

[27] Guido Mous. *A miniature chemical actuator with a compliant expansion chamber, passive exhaust valve and electrowetting-based fuel injection*. PhD thesis, Delft University of Technology, Delft, 11 2020.

[28] Chendong Guo, Zhengxing Zuo, Huihua Feng, Boru Jia, and Tony Roskilly. Review of recent advances of free-piston internal combustion engine linear generator. *Applied Energy*, 269:115084, 7 2020. ISSN 0306-2619. doi: 10.1016/J.APENERGY.2020.115084.

[29] Gurjinder Singh. Steady state and transient analysis of thermoelectric devices using finite element method. *RIT Rochester Institute of Technology*, 2003. URL https://scholarworks.rit.edu/theses/7068/.

[30] Henrik van den Heuvel. *Conceptual development of a catalytic expansion actuator for a resonating-body flapping-wing micro air vehicle*. PhD thesis, Delft University of Technology, Delft, 2 2015.

[31] Seyed Ehsan Hosseini. Micro-power generation using micro-turbine (moving) and thermophotovoltaic (non-moving) systems. *Proceedings of the Institution of Mechanical Engineers, Part A: Journal of Power and Energy*, 233(8), 12 2019. ISSN 0957-6509. doi: 10.1177/0957650919841958.

[32] HoSung Lee. *ME 5390 Advanced Thermal Design Course Literature (Chapter 2)*. Western Michigan University. URL ME5390AdvancedThermalDesign.

[33] S N Ivanov, P A Popov, G V Egorov, A A Sidorov, B I Kornev, L M Zhukova, and V P Ryabov. Thermophysical properties of aluminum nitride ceramic. *Physics of the Solid State*, 39(1):81–83, 1997. ISSN 1090-6460. doi: 10.1134/1.1129837. URL https://doi.org/10.1134/1.1129837.

[34] Jan Simon. ScaleTime, 2020. URL https://nl.mathworks.com/matlabcentral/fileexchange/25463-scaletime.

[35] Abdulrahman Jbaily and Ronald W Yeung. Piezoelectric devices for ocean energy: a brief survey. 1: 101–118. doi: 10.1007/s40722-014-0008-9.

[36] Yiguang Ju and Kaoru Maruta. Microscale combustion: Technology development and fundamental research. *Progress in Energy and Combustion Science*, 37(6):669–715, 12 2011. ISSN 0360-1285. doi: 10.1016/J.PECS.2011.03.001.

[37] Nam Il Kim, Souichiro Kato, Takuya Kataoka, Takeshi Yokomori, Shigenao Maruyama, Toshiro Fujimori, and Kaoru Maruta. Flame stabilization and emission of small Swiss-roll combustors as heaters. *Combustion and Flame*, 141(3):229–240, 5 2005. ISSN 0010-2180. doi: 10.1016/J.COMBUSTFLAME.2005.01.006.

[38] Nam Il Kim, Satoshi Aizumi, Takeshi Yokomori, Soichiro Kato, Toshiro Fujimori, and Kaoru Maruta. Development and scale effects of small Swiss-roll combustors. *Proceedings of the Combustion Institute*, 31 (2):3243–3250, 1 2007. ISSN 1540-7489. doi: 10.1016/J.PROCI.2006.08.077.

[39] C LEE. Design and fabrication of a micro Wankel engine using MEMS technology. *Microelectronic Engineering*, 73-74:529–534, 6 2004. ISSN 0167-9317. doi: 10.1016/J.MEE.2004.03.030.

[40] S A LLOYD and F J WEINBERG. A burner for mixtures of very low heat content. *Nature*, 251(5470):47–49, 1974. ISSN 1476-4687. doi: 10.1038/251047a0. URL https://doi.org/10.1038/251047a0.

[41] Melissa Fryer. FOULING IN HEAT EXCHANGERS, 2021. URL https://www.csidesigns.com/blog/articles/fouling-in-heat-exchangers#:~:text=Fouling%20is%20the%20formation%20of,flow%20resistance%20and%20pressure%20drops.

[42] L. Merotto, C. Fanciulli, R. Dondè, and S. De Iuliis. Study of a thermoelectric generator based on a catalytic premixed meso-scale combustor. *Applied Energy*, 162:346–353, 1 2016. ISSN 0306-2619. doi: 10.1016/J.APENERGY.2015.10.079.

[43] Anthony F. Mills. *HEAT AND MASS TRANSFER*. RICHARD D. IRWIN, INC., 1995.

[44] National Center for Biotechnology Information. Hydrogen peroxide. *PubChem Compound Summary for CID 784*. URL https://pubchem.ncbi.nlm.nih.gov/compound/Hydrogen-peroxide.

[45] B Preetham. *DEVELOPMENT OF A SMALL SCALE RESONANT ENGINE FOR MICRO AND MESOSCALE APPLICATIONS*. PhD thesis, 10 2014.

[46] B. S. Preetham, M. Anderson, and C. Richards. Modeling of a resonant heat engine. *Journal of Applied Physics*, 112(12), 2012. ISSN 00218979. doi: 10.1063/1.4769447.

[47] Olivier Riou, Pierre-Olivier Logerais, Vincent Froger, Jean-Félix Durastanti, and Anne Bouteville. Thermal study of an aluminium nitride ceramic heater for spray CVD on glass substrates by quantitative thermography. *Quantitative InfraRed Thermography Journal*, 10, 3 2013. doi: 10.1080/17686733.2013.793468.

[48] C R Roger, S H Yen, and K G Ramanathan. Temperature variation of total hemispherical emissivity of stainless steel AISI 304. *J. Opt. Soc. Am.*, 69(10):1384–1390, 10 1979. doi: 10.1364/JOSA.69.001384. URL https://opg.optica.org/abstract.cfm?URI=josa-69-10-1384.

[49] Christopher L. Seaman and Timothy R. Knowles. CARBON VELVET THERMAL INTERFACE GASKETS . Technical report, Energy Science Laboratories Inc., Reno, Nevada, 1 2001.

[50] Zu Guo Shen, Lin Li Tian, and Xun Liu. Automotive exhaust thermoelectric generators: Current status, challenges and future prospects. *Energy Conversion and Management*, 195:1138–1173, 9 2019. ISSN 0196-8904. doi: 10.1016/J.ENCONMAN.2019.05.087.

[51] Glen A. Slack, R. A. Tanzilli, R. O. Pohl, and J. W. Vandersande. The intrinsic thermal conductivity of AIN. *Journal of Physics and Chemistry of Solids*, 48(7):641–647, 1 1987. ISSN 0022-3697. doi: 10.1016/0022-3697(87)90153-3.

[52] Peter Stenzel, Manuel Baumann, Johannes Fleer, Benedikt Zimmermann, and Marcel Weil. Database development and evaluation for techno-economic assessments of electrochemical energy storage systems. In *2014 IEEE International Energy Conference (ENERGYCON)*, pages 1334–1342, 5 2014. doi: 10.1109/ENERGYCON.2014.6850596.

[53] Hugh S. Taylor. Catalysis. *Encyclopedia Britannica*, 7 2018. URL https://www.britannica.com/science/catalysis.

[54] The editors of Encyclopaedia. Seebeck effect, 11 1998. URL https://www.britannica.com/science/Seebeck-effect.

[55] S. Tijmons. *Autonomous Flight of Flapping Wing Micro Air Vehicles*. PhD thesis, Delft University of Technology, 12 2017.

[56] M. S. Tillack, A. R. Raffray, and J. E. Pulsifer. Improved Performance of Energy Recovery Ventilators Using Advanced Porous Heat Transfer Media. 12 2001.

[57] Tim van Wageningen. *Design analysis for a small scale hydrogen peroxide powered engine for a Flapping Wing Mechanism Micro Air Vehicle*. PhD thesis, Delft University of Technology, Delft, 1 2012.

[58] Y S Touloukian, P E Liley, and S C Saxena. Thermophysical Properties of Matter - The TPRC Data Series. Volume 3. Thermal Conductivity - Nonmetallic Liquids and Gases. *Defense Technical Information Center*, 1970.

[59] Bor Jang Tsai and Y. L. Wang. A novel Swiss-Roll recuperator for the microturbine engine. *Applied Thermal Engineering*, 29(2-3):216–223, 2 2009. ISSN 1359-4311. doi: 10.1016/J.APPLTHERMALENG.2008.02.028.

[60] Wolfgang Wagner, Hans-Joachim Kretzschmar, Roland Span, and Rolf Krauss. D2 Properties of Selected Important Pure Substances. In *VDI Heat Atlas*, pages 153–300. Springer Berlin Heidelberg, Berlin, Heidelberg, 2010. doi: 10.1007/978-3-540-77877-6{_}11.

[61] David C. Walther and Jeongmin Ahn. Advances and challenges in the development of power-generation systems at small scales. *Progress in Energy and Combustion Science*, 37(5):583–610, 9 2011. ISSN 0360-1285. doi: 10.1016/J.PECS.2010.12.002.

[62] Qi Wang. *Modeling, Design and Optimization of Flapping Wings for Efficient Hovering Flight*. PhD thesis, 6 2017.

[63] Sean Weera, Ho Sung Lee, and Alaa Attar. Utilizing effective material properties to validate the performance of thermoelectric cooler and generator modules. *Energy Conversion and Management*, 205:112427, 2 2020. ISSN 0196-8904. doi: 10.1016/J.ENCONMAN.2019.112427.

[64] Yang Wenming, Chou Siawkiang, Shu Chang, Xue Hong, and Li Zhiwang. Effect of wall thickness of micro-combustor on the performance of micro-thermophotovoltaic power generators. *Sensors and Actuators A: Physical*, 119(2):441–445, 4 2005. ISSN 0924-4247. doi: 10.1016/J.SNA.2004.10.005.

[65] J P Whitney and R J Wood. Conceptual design of flapping-wing micro air vehicles. *Bioinspiration & Biomimetics*, 7(3):036001, 9 2012. ISSN 1748-3182. doi: 10.1088/1748-3182/7/3/036001.

[66] Robert Wood, Radhika Nagpal, and Gu-Yeon Wei. Flight of the Robobees. *Scientific American*, 2013.

[67] S Woods, T Jung, D Sears, and J Yu. Emissivity of Silver and Stainless Steel from 80 K to 300 K: Application to ITER Thermal Shields. *Cryogenics*, 60, 11 2014. doi: 10.1016/j.cryogenics.2014.01.002.

[68] Yongjia Wu, Lei Zuo, Jie Chen, and Jackson A. Klein. A model to analyze the device level performance of thermoelectric generator. *Energy*, 115:591–603, 11 2016. ISSN 0360-5442. doi: 10.1016/J.ENERGY.2016.09.044.

[69] www.efunda.com. General Steam Table. URL https://www.efunda.com/Materials/water/steamtable_general.cfm.

[70] www.engineeringtoolbox.com. Water - Thermal Conductivity vs. Temperature. URL https://www.engineeringtoolbox.com/water-liquid-gas-thermal-conductivity-temperature-pressure-d_2012.html.

[71] Chen Xia, Zhiguang Zhang, Guoping Huang, and Yikai Xu. Study on the new hybrid thermodynamic cycle for an improved micro swing engine with heat recovery process. *Applied Thermal Engineering*, 129:1135–1149, 1 2018. ISSN 1359-4311. doi: 10.1016/J.APPLTHERMALENG.2017.10.123.

[72] W. M. Yang, S. K. Chou, C. Shu, H. Xue, Z. W. Li, D. T. Li, and J. F. Pan. Microscale combustion research for application to micro thermophotovoltaic systems. *Energy Conversion and Management*, 44(16):2625–2634, 9 2003. ISSN 0196-8904. doi: 10.1016/S0196-8904(03)00024-4.

[73] W. M. Yang, S. K. Chou, C. Shu, Z. W. Li, and H. Xue. Experimental study of micro-thermophotovoltaic systems with different combustor configurations. *Energy Conversion and Management*, 48(4):1238–1244, 4 2007. ISSN 0196-8904. doi: 10.1016/J.ENCONMAN.2006.10.002.

[74] Xiao Yang, Bo Yu, Xianyong Peng, and Huaichun Zhou. Investigation of thermal performance and energy conversion in a novel planar micro-combustor with four-corner entrances for thermophotovoltaic power generators. *Journal of Power Sources*, 515:230625, 12 2021. ISSN 0378-7753. doi: 10.1016/J.JPOWSOUR.2021.230625. URL https://linkinghub.elsevier.com/retrieve/pii/S0378775321011216.

[75] Xiao Yang, Bo Yu, Wenming Yang, and Huaichun Zhou. Investigation of heat transfer characteristics of hydrogen combustion process in cylindrical combustors from microscale to mesoscale. *International Journal of Hydrogen Energy*, 46(51):25893–25907, 7 2021. ISSN 0360-3199. doi: 10.1016/J.IJHYDENE.2021.05.099.

[76] Zhengyang Zhao, Zhengxing Zuo, Wei Wang, Ruiheng Liu, and Nianling Kuang. Performance optimization for a combustion-based micro thermoelectric generator with two-stage thermoelectric module. *Applied Thermal Engineering*, 198:117464, 11 2021. ISSN 1359-4311. doi: 10.1016/J.APPLTHERMALENG.2021.117464.

[77] Ze Guang Zhou, Dong Sheng Zhu, Yin Sheng Huang, and Chan Wang. Heat Sink Matching for Thermoelectric Generator. *Advanced Materials Research*, 383-390:6122–6127, 11 2011. ISSN 1662-8985. doi: 10.4028/www.scientific.net/AMR.383-390.6122.